



see commentary on page 974

OPEN

# Mitochondrial dysfunction and mitophagy blockade contribute to renal osteodystrophy in chronic kidney disease-mineral bone disorder

Shun-Neng Hsu<sup>1,2</sup>, Louise A. Stephen<sup>1</sup>, Kanchan Phadwal<sup>1</sup>, Scott Dillon<sup>1,9</sup>, Roderick Carter<sup>3</sup>, Nicholas M. Morton<sup>3,10</sup>, Ineke Luijten<sup>3</sup>, Katie Emelianova<sup>4,5,11</sup>, Anish K. Amin<sup>6</sup>, Vicky E. Macrae<sup>1,7</sup>, Tom C. Freeman<sup>1,12</sup>, Yu-Juei Hsu<sup>2</sup>, Katherine A. Staines<sup>8</sup> and Colin Farquharson<sup>1</sup>

<sup>1</sup>Division of Functional Genetics, The Roslin Institute and Royal (Dick) School of Veterinary Studies, University of Edinburgh, Easter Bush, Midlothian, UK; <sup>2</sup>Division of Nephrology, Department of Internal Medicine, Tri-Service General Hospital, National Defense Medical Center, Taipei, Taiwan; <sup>3</sup>Centre for Cardiovascular Science, Queen's Medical Research Institute, University of Edinburgh, Edinburgh, UK; <sup>4</sup>UK Dementia Research Institute, University of Edinburgh, Edinburgh Medical School, Edinburgh, UK; <sup>5</sup>Centre for Discovery Brain Sciences, Edinburgh Medical School, University of Edinburgh, Edinburgh, UK; <sup>6</sup>Edinburgh Orthopaedics, Royal Infirmary of Edinburgh, Edinburgh, UK; <sup>7</sup>School of Life Sciences, Faculty of Science and Engineering, Anglia Ruskin University, Cambridge, UK; and <sup>8</sup>Centre for Lifelong Health, School of Applied Sciences, University of Brighton, Brighton, UK

Chronic kidney disease-mineral and bone disorder (CKD-MBD) presents with extra-skeletal calcification and renal osteodystrophy (ROD). However, the pathophysiology of ROD remains unclear. Here we examine the hypothesis that stalled mitophagy within osteocytes of CKD-MBD mouse models contributes to bone loss. RNA-seq analysis revealed an altered expression of genes associated with mitophagy and mitochondrial function in tibia of CKD-MBD mice. The expression of mitophagy regulators, p62/SQSTM1, ATG7 and LC3, was inconsistent with functional mitophagy, and in mito-QC reporter mice with ROD, there was a two- to three-fold increase in osteocyte mitolysosomes. To determine if uremic toxins were potentially responsible for these observations, treatment of cultured osteoblasts with uremic toxins revealed increased mitolysosome number and mitochondria with distorted morphology. Membrane potential and oxidative phosphorylation were also decreased, and oxygen-free radical production increased. The altered p62/SQSTM1 and LC3-II expression was consistent with impaired mitophagy machinery, and the effects of uremic toxins were reversible by rapamycin. A causal link between uremic toxins and the development of

mitochondrial abnormalities and ROD was established by showing that a mitochondria-targeted antioxidant (MitoQ) and the charcoal adsorbent AST-120 were able to mitigate the uremic toxin-induced mitochondrial changes and improve bone health. Overall, our study shows that impaired clearance of damaged mitochondria may contribute to the ROD phenotype. Targeting uremic toxins, oxygen-free radical production and the mitophagy process may offer novel routes for intervention to preserve bone health in patients with CKD-MBD. This would be timely as our current armamentarium of anti-fracture medications for patients with severe CKD-MBD is limited.

*Kidney International* (2025) **107**, 1017–1036; <https://doi.org/10.1016/j.kint.2025.01.022>

KEYWORDS: autophagy; bone; CKD-MBD; mitophagy; renal osteodystrophy; uremic toxins

Copyright © 2025, International Society of Nephrology. Published by Elsevier Inc. This is an open access article under the CC BY-NC-ND license (<http://creativecommons.org/licenses/by-nc-nd/4.0/>).

**Correspondence:** Shun-Neng Hsu, Division of Nephrology, Department of Medicine, Tri-Service General Hospital, National Defense Medical Center, No. 325, Section 2, Cheng-Kung Road, Neihu District, Taipei, 114, Taiwan. E-mail: [h720127@gmail.com](mailto:h720127@gmail.com)

<sup>9</sup>Current affiliation: Yusuf Hamied Department of Chemistry, University of Cambridge, Cambridge, UK.

<sup>10</sup>Current affiliation: Centre for Systems Health and Integrated Metabolic Research, Department of Biosciences, School of Science and Technology, Nottingham Trent University, UK.

<sup>11</sup>Current affiliation: Department of Botany and Biodiversity Research, University of Vienna, Vienna, Austria.

<sup>12</sup>Current affiliation: Johnson and Johnson Innovative Medicine, Horsham, Pennsylvania, USA.

Received 14 January 2024; revised 10 January 2025; accepted 16 January 2025; published online 6 February 2025

## Translational Statement

Renal osteodystrophy (ROD) remains the major skeletal complication of chronic kidney disease–mineral and bone disorder (CKD-MBD). As a disease characterized by biochemical and hormone abnormalities, ROD is exacerbated by osteocyte mitochondrial dysfunction. The dysregulation of mitophagy in murine and human CKD-MBD bone provides evidence of delayed clearance of damaged mitochondria. Intervention studies with an antioxidant or a charcoal adsorbent mitigated the uremic toxin-induced mitochondrial changes and improved bone health. Understanding the mitophagy pathway better is vital to improving the clinical management of ROD. Furthermore, this study reveals the therapeutic potential of managing ROD by restoring defective mitophagy in osteocytes.

Chronic kidney disease–mineral and bone disorder (CKD-MBD) is a systemic disorder characterized by structural changes and the gradual loss of kidney function.<sup>1</sup> Diagnosis is strongly correlated with the increasing prevalence of diabetes and hypertension, as well as an aging population, and it is therefore a growing global health concern.<sup>2</sup> Progressive loss of kidney function leads to secondary hyperparathyroidism, hyperphosphatemia, and increased FGF23 levels. Through direct and indirect effects on bone-forming osteoblasts and bone-resorbing osteoclasts, this altered systemic milieu deregulates bone remodeling, mineral metabolism, and matrix mineralization, leading to compromised bone formation and ectopic calcification.<sup>3,4</sup> The skeletal complications of CKD-MBD are numerous and, based on bone morphology, often classified into a wide spectrum of bone disorders generically referred to as renal osteodystrophy (ROD).<sup>5</sup> Therapy often focuses on normalizing defective bone remodeling, but despite this, ROD often results in bone fractures, negatively impacting life quality and the survival of patients with renal disease.<sup>6,7</sup>

While most CKD-MBD studies have focused on the perturbation of mineral-regulating hormones, including PTH, FGF23, and vitamin D,<sup>8</sup> the complex bone–renal signaling pathways and cellular events they control during the development of ROD are unclear. Nevertheless, it is recognized that secondary hyperparathyroidism, particularly common in late-stage CKD-MBD, is associated with a net loss of bone mass despite an accelerating bone turnover.<sup>9</sup> This is a consequence of increased bone resorption through the upregulation of receptor activator of nuclear factor- $\kappa$ B ligand (RANKL) and the suppression of the RANKL decoy receptor, osteoprotegerin.<sup>10,11</sup> Retention of protein-bound uremic toxins such as indoxyl sulfate (IS) and p-cresyl sulfate (PCS) in the circulation and organs of patients with CKD also affects bone quality.<sup>12,13</sup> Uremic toxins induce oxygen free radical production by mitochondria, and the resultant oxidative stress disrupts bone quantity and quality due to the unfavorable effects on osteoblasts and osteoclasts and matrix mineralization.<sup>12,14</sup> Uremic toxins also reduce the number of osteoblast PTH receptors, and the resultant skeletal resistance to PTH may explain the dynamic bone disease during the early stages of CKD-MBD.<sup>15</sup>

Our inadequate understanding of the etiology of ROD drove us to complete a series of studies aimed at providing insight into the cellular mechanism(s) responsible. The identification of dysregulated mitophagy by uremic toxins and the accumulation of damaged mitochondria in osteocytes may help identify novel therapeutic options to manage skeletal complications in patients with renal disease.

## METHODS

CKD-MBD was induced using dietary adenine supplementation or 5/6 nephrectomy (5/6 Nx) in 8-week-old male C57BL/6J and *mito*-QC mice and analysis involving gene expression (RNA-sequencing [RNA-seq]), mitophagy assessment (mitolysosome quantification, immunoblotting, and

immunofluorescence) and radiographic imaging (micro-computed tomography) were completed in skeletal tissue. Intervention studies with mitoquinone (MitoQ; Abcam) and AST-120 (Kremezin®; Kureha Corporation) were also completed as were studies of bones from human patients with CKD-MBD. Osteoblasts isolated from wild-type and *mito*-QC pups were challenged by IS and PCS and mitochondrial morphology, mitophagy regulators, reactive oxygen species (ROS) production, and respiration and glycolysis were examined. Quantification of mitolysosomes, gene expression, and matrix mineralization were completed with osteoblasts isolated from adult CKD-MBD *mito*-QC mice. Full methods are found in the [Supplementary Methods](#).

## RESULTS

### Dietary adenine-supplemented mice develop a ROD phenotype

Mice fed an adenine-supplemented diet presented with a serum profile and skeletal phenotype typical of CKD-MBD and ROD, respectively. CKD-MBD mice began losing body weight by day 5 ([Figure 1b](#)) and presented with hyperphosphatemia, hyperparathyroidism, and increased serum blood urea nitrogen, creatinine, calcium, and FGF23 levels ([Figure 1c](#)) relative to control (CTL) mice. The higher FGF23 levels likely reflect the hyperphosphatemia but inflammation, a common complication of CKD is known to occur in adenine-fed rodents, also raises FGF23 levels.<sup>16</sup> Overall, the altered serum profile of mice offered the adenine-supplemented diet, which is associated with increased bone remodeling, corresponds to an advanced stage of human CKD.<sup>17,18</sup> Bone structure and biomechanical properties were also compromised in CKD-MBD mice and presented with a typical ROD phenotype ([Supplementary Figure S1A–D](#)). We next completed an RNA-seq analysis to identify changes to the bone transcriptome during the development of ROD.

### Experimental ROD is associated with clusters of differentially expressed genes

A Pearson correlation ( $r \geq 0.98$ ) matrix was constructed to define relationships between samples using Graphia.<sup>19</sup> The 3-dimensional visualization ([Figure 2a](#)) of the correlation between the individual sample groups identified CTL samples ( $n = 12$ ) in the periphery and CKD-MBD samples ( $n = 28$ ) in a more central position within the major cluster. Unexpectedly, CKD-MBD samples were less heterogeneous than CTL samples, suggesting reduced bone cell activity. Principal component analyses disclosed that the first 2 principal components (PC1 + PC2) explained 56.1% of the data variance ([Figure 2b](#)).

A gene-to-gene correlation network was generated with a Pearson correlation threshold ( $r \geq 0.85$ ) and a Markov clustering inflation value of 1.6 was used to define relationships between genes. The correlation network comprised nodes (genes) correlated with CKD-MBD after enrichment analysis and the formation of clusters of differentially expressed genes from day 20 and day 35 samples ([Figure 2c](#)). The network included 3,455 nodes and 730,900 edges (links).

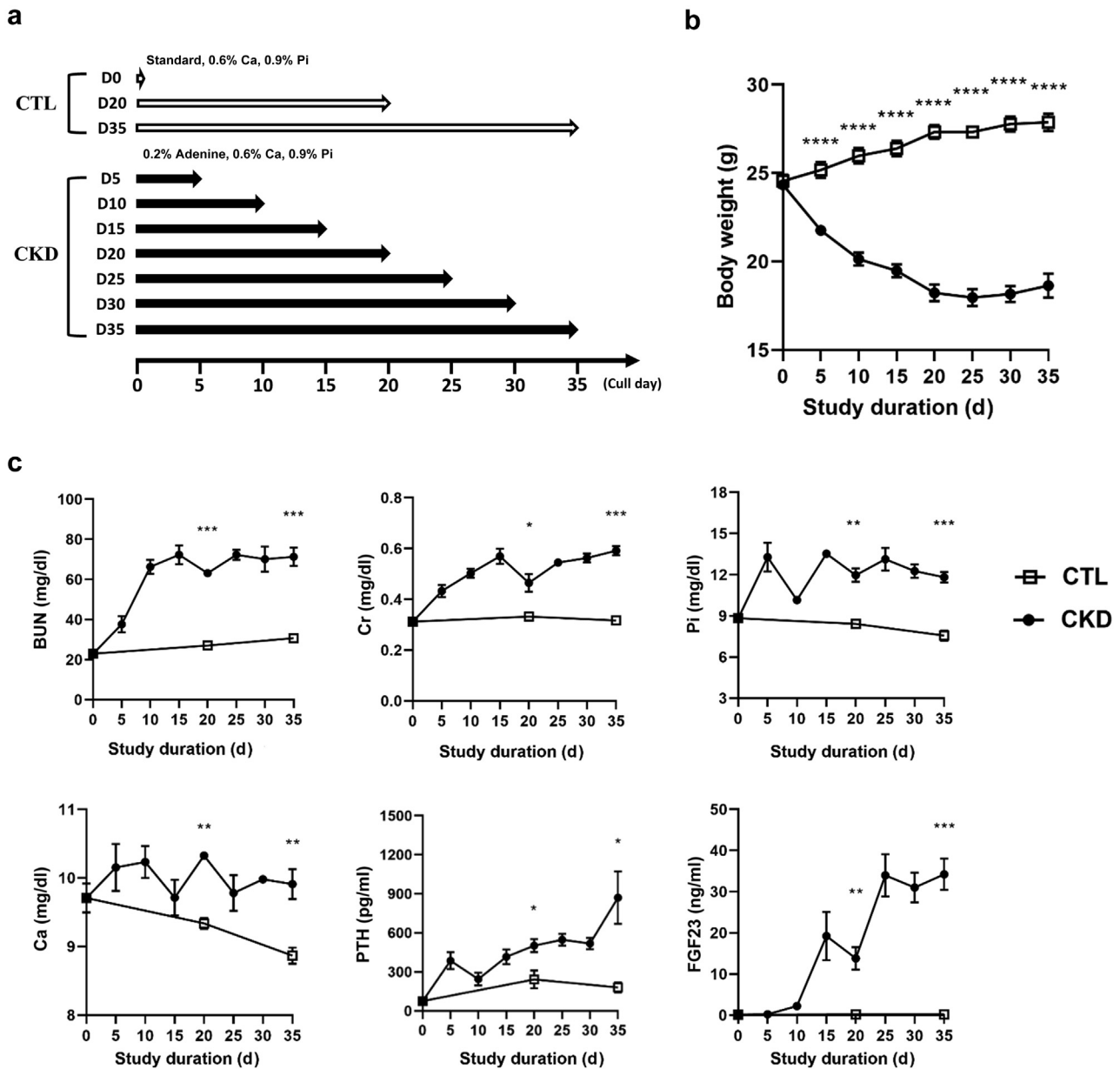


**Figure 1 | Experimental design for RNA-sequencing study and time-dependent changes in body weight and serum biochemistries in the adenine-induced mouse model.** (a) Forty 8-week-old male C57BL/6J mice were randomly allocated into 10 groups of 4 mice to the control (CTL) group ( $n = 12$ ) and sacrificed after day 0 (D0), D20, and D35 or the chronic kidney disease–mineral and bone disorder (CKD-MBD) group ( $n = 28$ ) and sacrificed every 5 days from D5 to D35. (b) Body weight progressively decreased in the CKD-MBD mice, which began losing weight by D5, plateauing at  $\sim$ D25. (c) Serum levels of blood urea nitrogen (BUN), creatinine (Cr), calcium (Ca), inorganic phosphate (Pi), PTH, and FGF23 were all increased in the CKD-MBD mice sacrificed at each sampling point. The data are represented as mean  $\pm$  SEM ( $n = 4$ ). \* $P < 0.05$ , \*\* $P < 0.01$ , \*\*\* $P < 0.001$ , and \*\*\*\* $P < .0001$  versus CTL mice of the same age. NS, not significant.

Two distinct groups of nodes sharing the same correlation factor were selected for functional analysis. The top representative group ( $\geq 1.5$ -fold upregulated) contained 411 transcripts whose expression was upregulated in bones from CKD-MBD mice. In contrast, the bottom group ( $\leq 1.5$ -fold downregulated) had 754 transcripts downregulated in bones from CKD-MBD mice. All other genes identified within both groups were highly correlated and consistently down- or

upregulated across all time points of CKD-MBD mice but did not reach the 1.5-fold threshold. The smallest cluster size of the 2-node algorithm was used to subdivide the network into discrete gene clusters that contained genes with similar biological functions and expression patterns over time. For example, the expression profiles of the 5 genes in the *Fgf23* cluster (cluster 16) are shown in Figure 2d and Supplementary Figure S2.

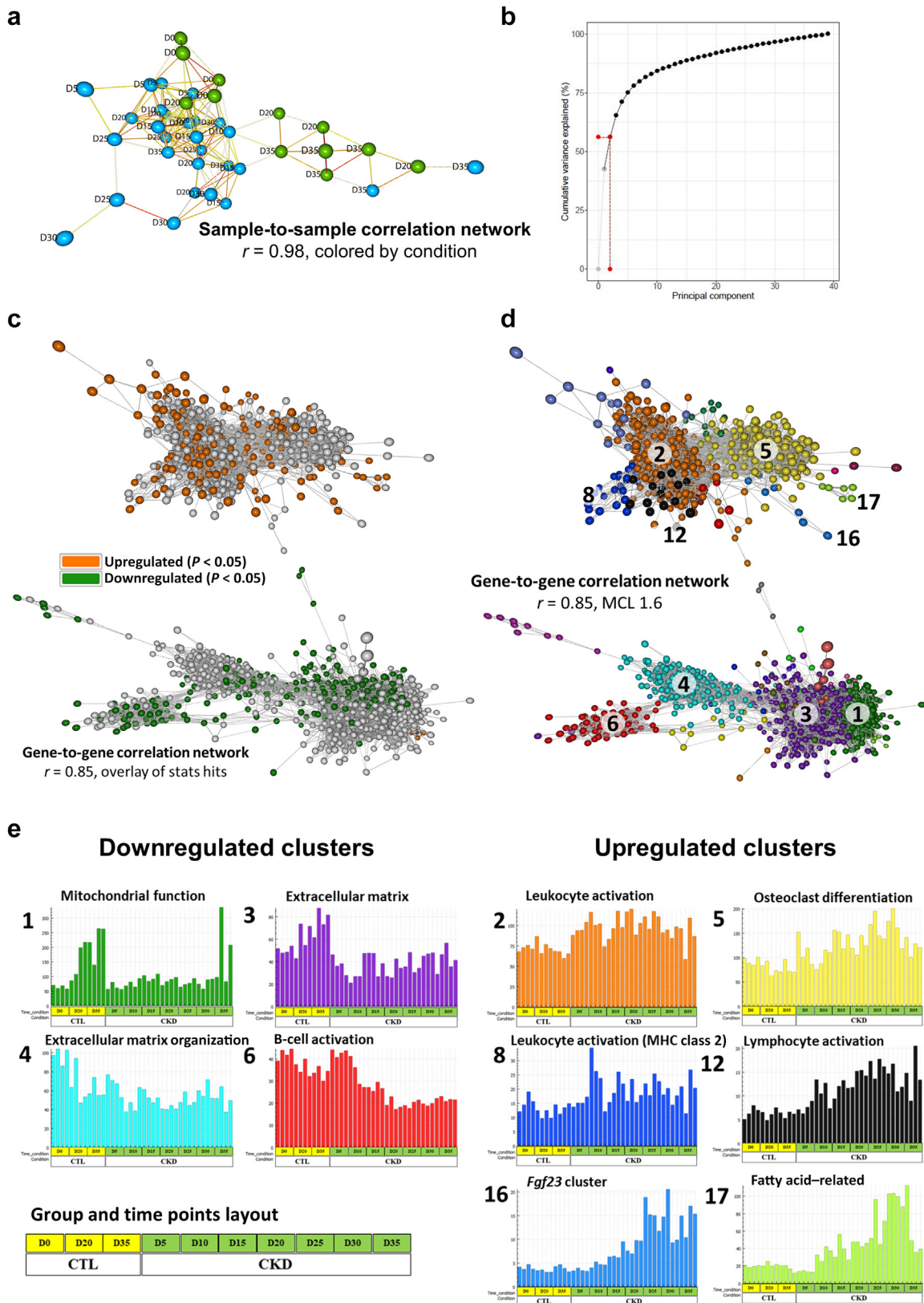


**Figure 2 | Network visualization and analysis reveal chronic kidney disease–mineral and bone disorder (CKD-MBD) correlated gene clusters with bespoke biological functions.** (a) Three-dimensional visualization of a sample-to-sample Pearson correlation network of control samples ( $n = 12$ , green nodes) and CKD samples ( $n = 28$ , blue nodes) showed late time points to be generally more distinct from early time points and, for the most part, control samples to be different from CKD samples. The strength of edges (line) was represented on a scale from thin and blue (weak) to thick and red (strong). It corresponded to correlations between individual measurements above the (continued)

### The expression of genes associated with mitochondrial function is altered in ROD

The resultant correlation network comprised 41 gene clusters related to the development of ROD; there were 17 clusters of upregulated genes and 24 clusters of downregulated genes (Figure 2d). Of the 41 clusters, 10 possessed biological functions associated with bone metabolism/(re)modelling, and additional functional enrichment analysis using ToppGene (<https://toppgene.cchmc.org/>) identified the biological process associated with the genes in each of these 10 clusters (Figure 2e). The development of ROD was associated with leukocyte and lymphocyte activation (clusters 2, 8, and 12) and the suppression of B-cell function (cluster 6), which confirms that CKD is a chronic inflammatory state.<sup>20</sup> Increased osteoclast differentiation (cluster 5) and altered extracellular matrix structure and organization (clusters 3 and 4) were consistent with increased bone (re)modelling during the development of ROD.<sup>21,22</sup> Similarly, increased bone marrow fat and *Fgf23* expression are recognized hallmarks of CKD-MBD.<sup>23,24</sup> An unexpected finding was the downregulation of genes associated with mitochondrial function and energy metabolism (cluster 1) during the development of ROD (Figure 2e).

### Identification of mitochondrial pathways downregulated in ROD

To identify mitochondrial and energy-related pathways implicated in the etiology of ROD, we performed WebGestalt (Zhang Lab) enrichment analyses on the genes within cluster 1 (Figure 3a). The top 10 gene ontology terms identified included the tricarboxylic acid cycle, oxidative phosphorylation, and neurodegenerative disorder-associated pathways. Heatmaps identified genes in cluster 1 that were downregulated in pathways associated with glycolysis and mitochondrial function, such as the tricarboxylic acid cycle, mitophagy, and mitochondrial electron transport chain complexes I to IV (Figure 3b). The expression of mitophagy-associated genes in CKD-MBD samples did not, unlike CTL samples, increase over the experimental period. Similar changes to the mitochondrial transcriptome and mitoproteome during postnatal development of the murine heart

have also been noted.<sup>25</sup> There was a rapid increase in the expression of oxidative phosphorylation proteins between 8 and 12 weeks of age. Furthermore, the downregulation of mitochondrial gene expression was a hallmark of mitochondrial dysfunction in the mouse heart.

### Mitolysosomes are increased in osteocytes of ROD mice

We speculated that a reduced clearance of damaged mitochondria detected in experimental ROD could underpin the downregulation of energy production pathways in mitochondria.<sup>26</sup> Therefore to quantify mitophagy within osteocytes (the most abundant cell type in bone and the likely source of the RNA-seq transcriptome data), we induced CKD-MBD in *mito-QC* mice. There was a 2- to 3-fold increase in red puncta (mitolysosomes, i.e., degraded mitochondrial components within lysosomes, as an index of mitophagy<sup>27</sup>) in cortical bone osteocytes of CKD-MBD mice (Figure 4a–c). The accumulation of osteocyte mitolysosomes in ROD could indicate either enhanced mitophagy activation or a blockage of downstream steps in mitochondria removal. Interestingly, the dendritic processes radiating from the osteocyte cell body were reduced in CKD-MBD mice, which may impede the endoplasmic reticulum-mediated removal of defective osteocyte mitochondria in ROD (Supplementary Figure S3).<sup>28</sup> Increased mitolysosomes in CKD-MBD were also observed in the renal tubules and glomeruli of CKD-MBD mice (Supplementary Figure S4).

### The expression of mitophagy regulatory proteins in osteocytes from CKD-MBD bone suggests a block in the clearance of damaged mitochondria

To identify the mechanisms leading to mitolysosome accumulation in ROD, the expression of established mitophagy regulators was analyzed (Figure 5). The expression of PARKIN, an E3 ubiquitin ligase that promotes mitophagy, was increased in cortical bone from CKD-MBD mice (Figure 5a and b). The autophagic adaptor protein, p62 (SQSTM1) is a major light chain 3 (LC3)-II (recruits selective cargo to the autophagosome) interacting protein and as a selective substrate it is normally degraded during autophagy.<sup>29</sup> This was not found in this study. Immunostaining revealed increased

**Figure 2 |** (continued) defined threshold ( $r \geq 0.98$ ). **(b)** The red line indicated that the first 2 principal components (PC1 + PC2) explain 56.1% of the variance of the data. **(c)** A coexpression graph of the RNA-sequencing data was constructed composed of 3,455 nodes (genes) and 730,900 edges (correlations  $r \geq 0.85$ ). The graph was made up of 2 large and unconnected components of genes representing those whose expression was higher or lower in the CKD samples relative to controls (CTL) as seen when differentially expressed genes with  $\geq 1.5$ -fold change from day 20 (D20) and D35 samples were overlaid on the network. The group highlighted in orange contains 411 transcripts whose expression was significantly upregulated following adenine-induced CKD-MBD at D20 and D35. The group highlighted in green includes 754 transcripts consistently downregulated following adenine-induced CKD-MBD at D20 and D35. **(d)** The network's nodes represent CKD-MBD correlated genes, and edges represent correlations above a defined threshold ( $r \geq 0.85$ ). Coexpressed genes form highly connected complex clusters within the graph. A gene-to-gene correlation graph was generated from all genes that were correlated ( $r \geq 0.85$ ) with differentially expressed genes from D20 and D35 (CKD vs. control). Nodes were colored by cluster using the Markov clustering (MCL) algorithm (1.6) according to their specific biological function. The edges corresponded to the correlation between them. **(e)** Ten histograms showing the mean expression profile of gene clusters. Further functional enrichment analysis identified the biological processes associated with the genes in each of these 10 clusters. Those associated with *Fgf23* function, osteoclast differentiation, fatty acid synthesis, and leukocyte and lymphocyte activation increased with time, whereas genes associated with mitochondria function, B-cell activation, and extracellular matrix structure and organization decreased over time. MHC, major histocompatibility complex.

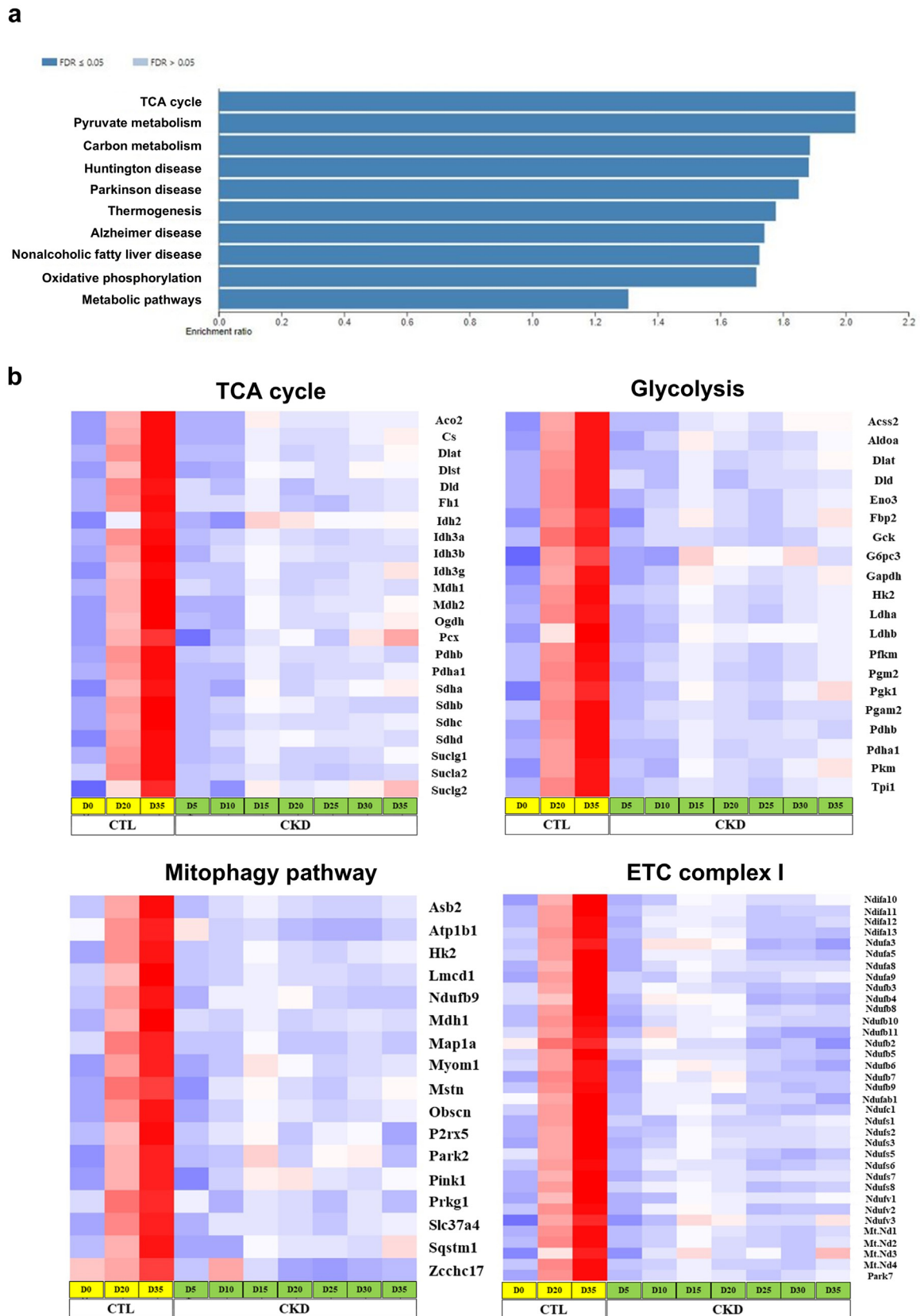


**Figure 3 | Pathway analysis of differentially expressed genes in cluster 1 of the RNA-sequencing data. (a)** The top 10 gene ontology terms are listed. **(b)** Heatmaps were derived from the average value of 4 biological replicates at each time point and showed that genes associated with the tricarboxylic acid (TCA) cycle, glycolysis, mitophagy, and electron transport chain (ETC) complex I (and II, III, and IV [not shown]) were downregulated in chronic kidney disease (CKD)–mineral and bone disorder mouse bones. CTL, control; D0, day 0.

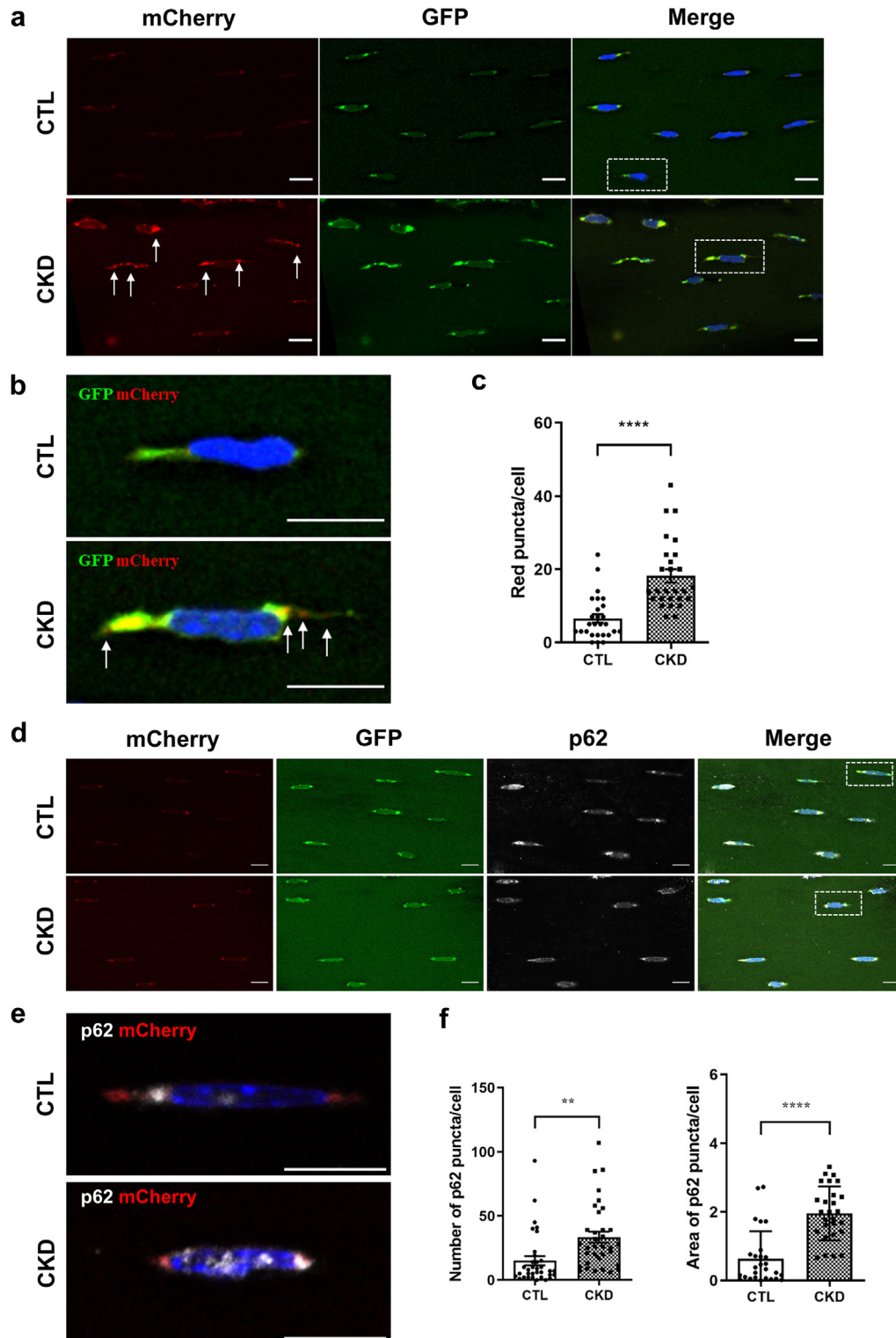


**Figure 4 | Quantification of mitophagy in osteocytes of cortical bone from adenine-fed mice.** (a) Cortical bones from control (CTL) and Chronic kidney disease–mineral and bone disorder (CKD-MBD) *mito-QC* mice were imaged, whereby significant red mitophagic puncta were identified in osteocytes of CKD-MBD bones (white arrows). (b) Red mitophagic puncta (white arrows) were observed at higher magnification within the osteocyte cytoplasm and emerging dendrites. (c) Red mitophagic puncta were increased in the CKD-MBD mice. Each dot represents the total number of red puncta per osteocytes (9 osteocytes per 5 sections per mouse;  $n = 3$ ). (d) Assessment of the selective autophagy adaptor p62/SQSTM1 in CTL and CKD *mito-QC* mice osteocytes. (e) Representative images of white p62 colocalized with red mitolysosomes showing p62 accumulation in CKD osteocytes. (f) The average number and area ( $\mu\text{m}^2$ ) of p62 colocalized puncta per osteocyte were increased in CKD-MBD bones. Each dot represents the average number and surface area of the colocalized puncta per cell (9 osteocytes per 5 sections per mouse,  $n = 3$ ). Bar = 10  $\mu\text{m}$ . Data are presented as mean  $\pm$  SEM. Analysis was tested by Student's *t* test. \*\* $P < 0.01$  and \*\*\*\* $P < 0.0001$  versus the CTL group. GFP, green fluorescent protein. To optimize viewing of this image, please see the online version of this article at [www.kidney-international.org](http://www.kidney-international.org).

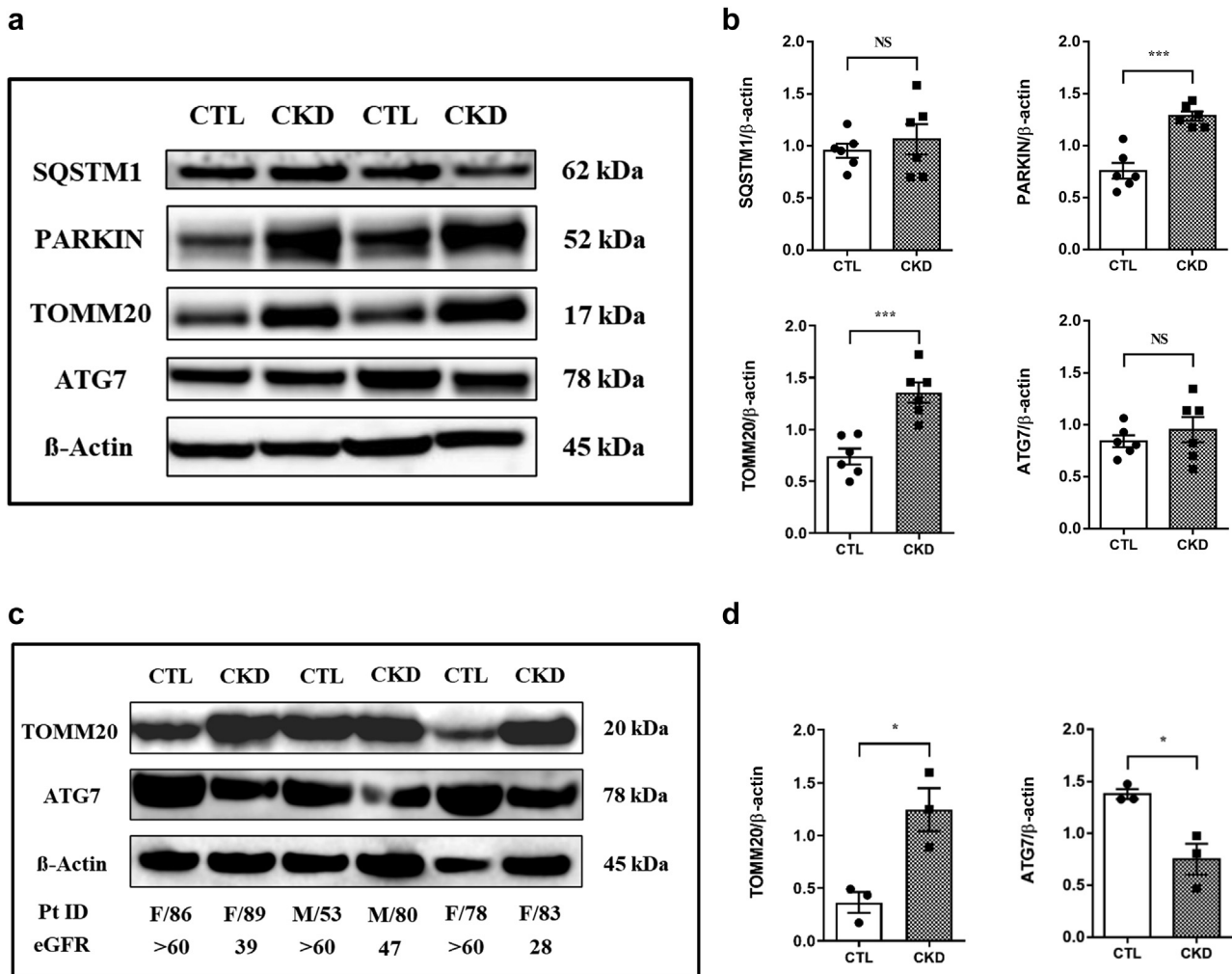


**Figure 5 | Mitophagy regulators are altered in the femurs of chronic kidney disease–mineral and bone disorder (CKD-MBD) mice and patients.** (a) Representative Western blots of 2 control (CTL) and 2 CKD-MBD samples showing protein expression levels of mitophagy-associated proteins in cortical bone of mouse femurs. (b) Quantification of SQSTM1, PARKIN (an E3 ubiquitin ligase that promotes mitophagy), TOMM20 (a subunit of the mitochondrial translocase of the outer membrane complex), and ATG7 Western blot protein levels in cortical bone from CTL and CKD-MBD mouse femurs. The expression of both PARKIN and TOMM20 were increased in the CKD-MBD mice. (c,d) Western blot analyses and quantification of TOMM20 and ATG7 in cortical bone of human femurs (n = 3). The expression of both TOMM20 and ATG7 were increased in the CKD-MBD bone. Data are presented as means ± SEM. Analysis was tested by Student’s t test. \*P < 0.05 and \*\*\*P < 0.001 versus the CTL group. eGFR, estimated glomerular filtration rate; F, female; M, male; NS, not significant; Pt ID, patient ID.

numbers of p62/SQSTM1 puncta in osteocytes of *mito-QC* CKD-MBD mice (Figure 4d–f) that concurred with a similar trend in p62/SQSTM1 expression as detected by immunoblotting (Figure 5a and b). Also, ATG7, which increases during autophagy and is involved in autophagosome biogenesis through the lipidation of LC3-I to LC3-II, was similarly expressed in bone from CTL and CKD-MBD mice (Figure 5a and b). These observations are incongruous with increased mitophagy and suggest a block in the removal of damaged mitochondria via the autophagic machinery. Increased osteocyte mitochondria number was confirmed using the mitochondrial marker TOMM20, a subunit of the mitochondrial translocase of the outer membrane complex, supporting the concept that mitochondria are not being cleared in ROD (Figure 5a and b). This was replicated in the

cortical bone of patients with CKD-MBD, whereas a decrease in ATG7 levels was observed (Figure 5c and d).

**Confirmation of disrupted mitophagy in the 5/6 Nx model**

Dietary adenine supplementation may induce toxic effects that are not limited to the kidney and may explain the noted rapid body weight loss. To rule out potential confounding factors as a cause of the observed altered mitophagy we established the 5/6 Nx model in *mito-QC* mice. The 5/6 Nx mice had similar food intake, final body weight, and tibial length as the sham CTL mice (Figure 6a). The serum profile and bone phenotype were typical of CKD-MBD and ROD, respectively, and the number of mitolysosomes within cortical bone osteocytes was increased in the 5/6 Nx mice (Figure 6b–e). These data from a second animal model provide

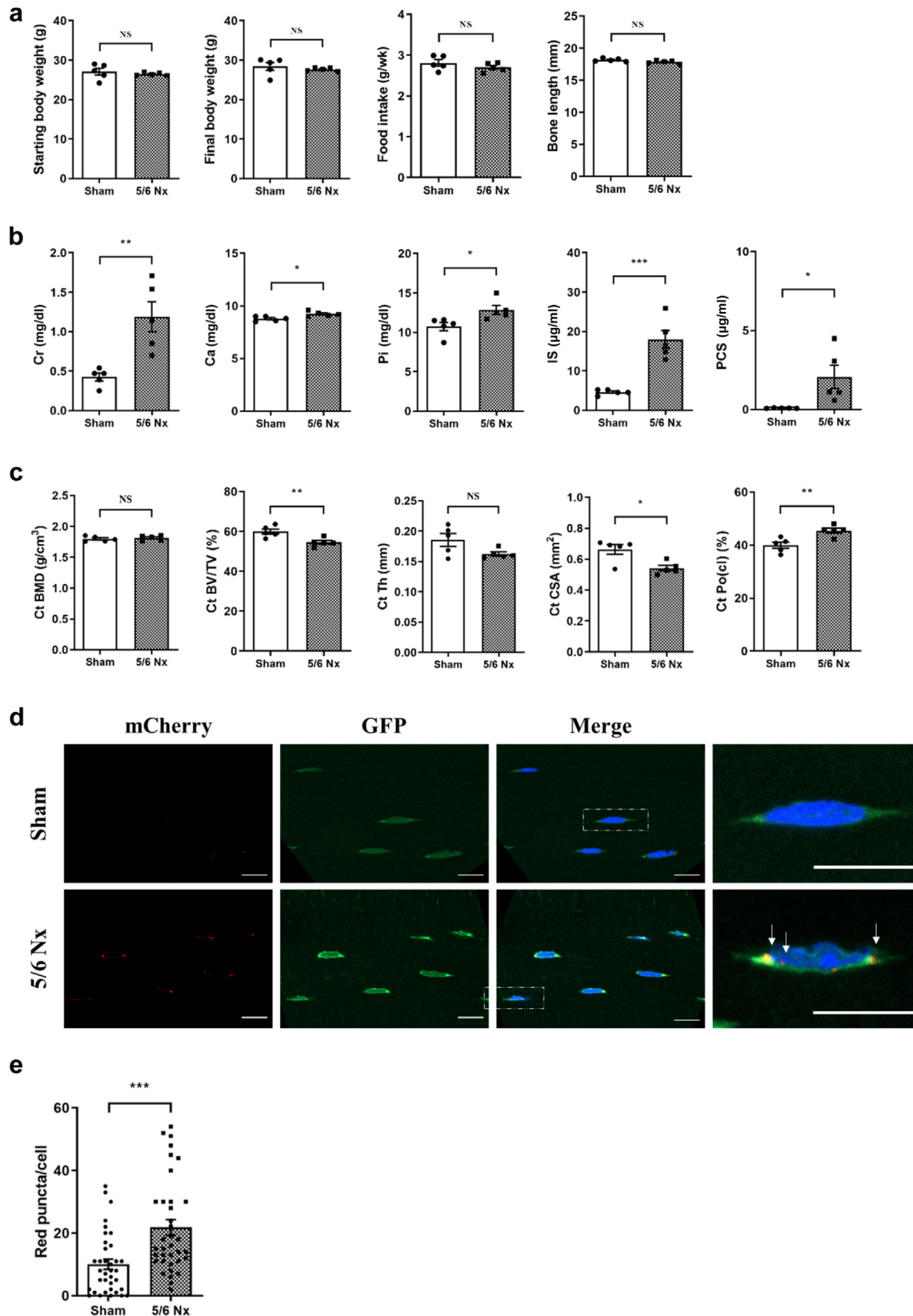


**Figure 6 | Mitophagy dysfunction in osteocytes from the 5/6 nephrectomy (5/6 Nx) mouse model.** (a) Weekly food intake and final body weight and tibial length were similar in sham-operated and 5/6 Nx mice ( $n = 5$ ). (b) Serum levels of creatinine (Cr), calcium (Ca), inorganic phosphate (Pi), indoxyl sulfate (IS), and p-cresyl sulfate (PCS) were higher in 5/6 Nx mice ( $n = 5$ ). (c) The 5/6 Nx mice exhibited decreased cortical (Ct) bone volume/tissue volume (Ct BV/TV), thickness (Ct Th), and cross-sectional area (Ct CSA) but increased closed (continued)

reassurance that mitochondrial dysfunction is a direct consequence of CKD-MBD.

#### Establishment of a causal link among uremic toxins, mitochondrial dysfunction, and ROD

To establish whether a causative link exists between mitochondrial dysfunction and the development of ROD, CKD-MBD mice were administered the mitochondrial-targeted antioxidant, MitoQ. MitoQ did not prevent reductions in body weight, food intake, or tibial length but serum inorganic phosphate and PCS, and urine neutrophil gelatinase-associated lipocalin-creatinine (NGAL/Cr) ratio were reduced (Figures 7a and b and 8a). However, while serum creatinine, a measure of renal function, worsened with MitoQ, cortical bone loss and porosity were lessened and the increase in osteocyte mitolysosomes was mitigated (Figures 7c and 8b and c). Furthermore, the addition of charcoal absorbent AST-120 to the diet of adenine-fed mice prevented body weight loss, normalized serum creatinine, calcium, inorganic phosphate, IS, and PCS and reduced the bone changes characteristic of ROD (Figure 7d–f). AST-120 also resulted in improved renal function and an osteocyte mitolysosome number that was similar to that of the CTL mice (Figure 8a–c). The MitoQ and AST-120 data provide strong evidence for a causal link among uremic toxins levels, mitochondrial changes, and the development of ROD.

#### IS impairs mitochondria function, morphology, and mitophagy in osteoblasts

Uremic toxins accumulate in body fluids during progressive CKD and may induce mitochondrial damage and impair autophagy.<sup>30,31</sup> Therefore, the failure to remove damaged mitochondria via impaired mitophagy (Figures 4 and 5a–d) may result from increased uremic toxin levels in CKD-MBD mice (Figures 6b and 7b and e). To examine this, osteoblasts were treated with the uremic toxin, IS (0–2 mmol/l) for 7 days, a treatment regimen that was not toxic to cells (Supplementary Figure S5). Osteoblast mitochondrial  $\Delta\Psi$  was decreased by IS as evidenced by a reduction in mitotracker red uptake, which is dependent on  $\Delta\Psi$ , whereas IS treatment increased mitochondrial and cellular ROS production in a concentration-dependent manner (Figure 9a–c). In CTL cells, the mitochondrial network appeared as long thread-like tubular structures distributed throughout the cytoplasm, whereas in the IS-treated cells the mitochondrial network was disintegrated and characterized by fragmented mitochondria with a swollen rounded morphology, collapsed around the nuclei (Figure 9d). Determination of mitochondrial oxygen consumption rate and extracellular acidification rate revealed that basal and maximum respiration and

glycolysis capacity were decreased by IS, as was ATP production, maximum  $H^+$  leak, and nonrespiratory oxygen consumption rate (Figure 10a–c). Finally, p62/SQSTM1 expression was upregulated by IS treatment in a concentration-dependent manner, whereas the expression of PARKIN and autophagic marker LC3-II (generated in an ATG7-dependent manner) were downregulated by IS (Figure 11a and b and Supplementary Figures S6 and S7).

#### Rapamycin rescues osteoblasts from the adverse effects of IS on mitochondrial morphology and clearance, ROS production, and mitophagy

Rapamycin, a specific mammalian target of rapamycin inhibitor, is an autophagy inducer that increases oxidative phosphorylation, decreases ROS production, and, by removing damaged or dysfunctional mitochondria, it improves overall mitochondrial quality.<sup>32,33</sup> Cells ( $\pm$  IS) were treated with vehicle (control) or rapamycin ( $\pm$  Rapa) for 7 days, and it was found that the reduction of PARKIN expression and the reduced conversion of LC3-I to LC3-II by IS was prevented by rapamycin (Figure 11c and d and Supplementary Figure S6).

Rapamycin also partly reversed the IS-increased p62/SQSTM1 expression (Figure 11c and d and Supplementary Figure S7). Furthermore, the oxidative stress induced by IS was lowered by coinubation with rapamycin and the ability of rapamycin to reactivate IS-suppressed mitophagy and efficiently remove damaged mitochondria resulted in the correction of the abnormal morphology and distribution of mitochondria (Figure 9e and f). These results imply that rapamycin could rescue osteoblasts from the adverse effects of IS on mitochondria morphology and mitophagy.

#### MitoQ mitigates the effects of PCS on osteoblast mitolysosome number

To ensure the osteoblast response to IS was typical of uremic toxins, we also examined the effects of PCS, another uremic toxin that was elevated in the serum of CKD-MBD mice (Figures 6b and 7b and e). PCS induced osteoblast mitolysosome number and this increase was mitigated by supplementation of the culture medium by MitoQ (Figure 12).

#### Osteoblasts isolated from CKD-MBD mice show mitochondrial abnormalities and altered differentiation and mineralization capabilities

To determine whether osteoblasts with mitochondrial dysfunction have impaired differentiation and matrix mineralization potential, osteoblasts were isolated from CKD *mito*-QC mice (adenine and 5/6 Nx models) and studied *ex vivo*. Compared to control osteoblasts, mitolysosome number was higher in osteoblasts isolated from both animal

**Figure 6 |** (continued) porosity [Po (cl)] (n = 5). **(d,e)** Representative immunofluorescence images of *mito*-QC mice revealed an increase in red mitophagic puncta (white arrows) in osteocytes from 5/6 Nx mice. The quantification of red mitophagic puncta is shown, and each dot represents the total number of red puncta per cell. Bars = 10  $\mu$ m (9 osteocytes per 5 sections per mouse, n = 4). Data are presented as mean  $\pm$  SEM. Analysis was tested by Student's *t* test. \**P* < 0.05; \*\**P* < 0.01; \*\*\**P* < 0.001 versus the sham group. GFP, green fluorescent protein; NS, not significant. To optimize viewing of this image, please see the online version of this article at [www.kidney-international.org](http://www.kidney-international.org).

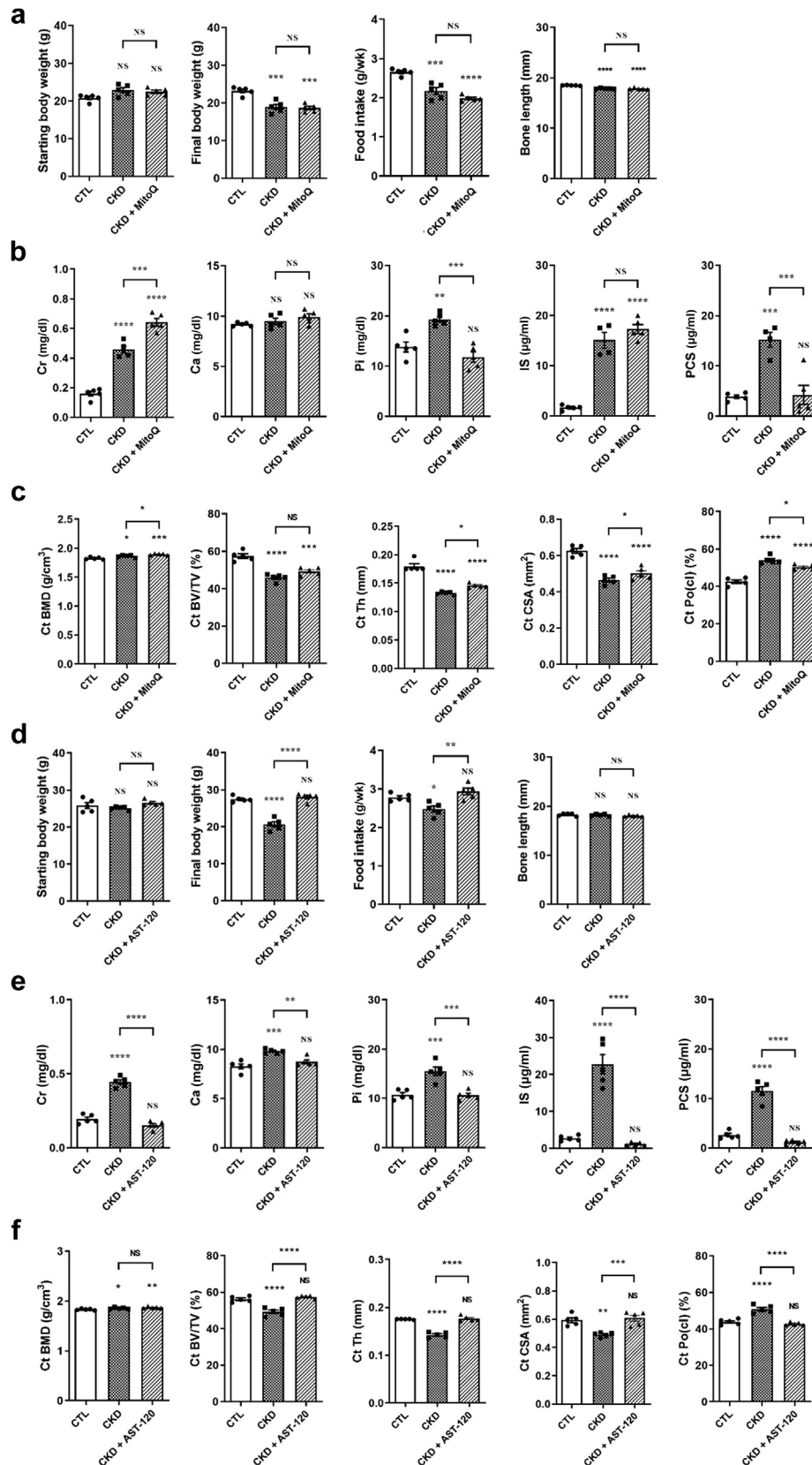


**Figure 7 | Effects of MitoQ and AST-120 on bone and serum markers in the adenine-induced chronic kidney disease (CKD) mouse model.** (a) Weekly food intake and final body weight and tibial length were all decreased in the chronic kidney disease–mineral and bone disorder (CKD-MBD) mice and MitoQ i.p. treatment did not prevent these changes. (b) MitoQ prevented the increase in serum inorganic phosphate (Pi) and p-cresyl sulfate (PCS) levels in the CKD-MBD mice. (c) MitoQ improved cortical (Ct) bone volume/tissue (continued)

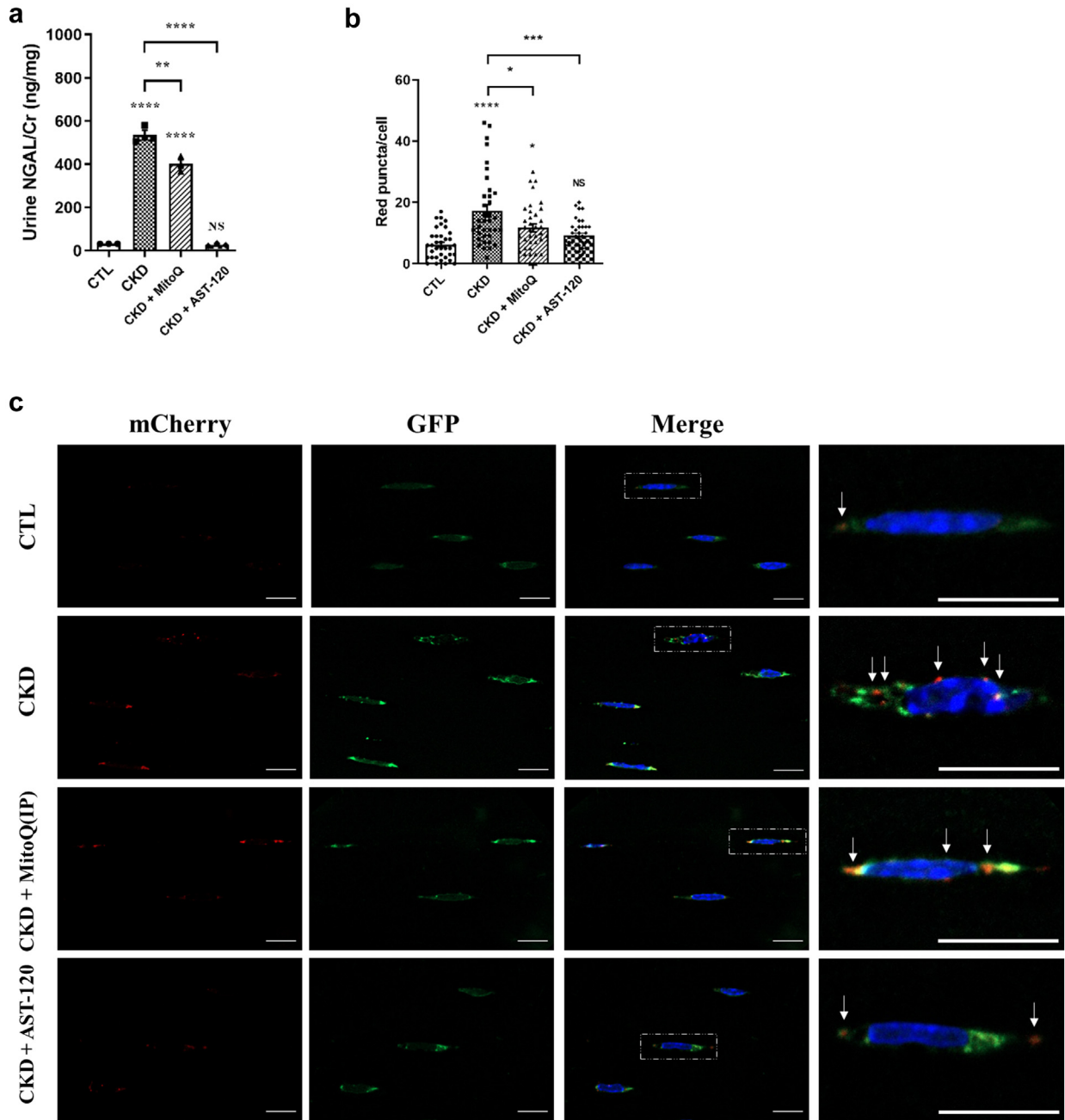


**Figure 8 | Impact of MitoQ and AST-120 on osteocyte mitophagy and renal function in adenine-induced chronic kidney disease (CKD).** (a) The increased urine neutrophil gelatinase–associated lipocalin–creatinine (NGAL/Cr) ratio in chronic kidney disease–mineral and bone disorder (CKD-MBD) mice was lowered by MitoQ and AST-120 ( $n = 3$ ). (b) CKD-MBD mice had an increased number of mitolysosomes that was attenuated by MitoQ and AST-120 treatment. (c) Representative images of mitolysosomes in osteocytes from sections of control (CTL), CKD, CKD + MitoQ, and CKD + AST-120–treated mice. The quantification of red mitophagic puncta (white arrows) is shown, and each dot represents the total number of red puncta per osteocytes (9 osteocytes per 5 sections per mouse,  $n = 4$ ). Bar = 10  $\mu\text{m}$ . Data are presented as means  $\pm$  SEM. Analysis was tested by 1-way analysis of variance. \* $P < 0.05$ , \*\* $P < 0.01$ , \*\*\* $P < 0.001$ , and \*\*\*\* $P < 0.0001$  versus the CTL group. GFP, green fluorescent protein; NS, not significant. To optimize viewing of this image, please see the online version of this article at [www.kidney-international.org](http://www.kidney-international.org).

**Figure 7 |** (continued) volume (Ct BV/TV), thickness (Ct Th), cross-sectional area (Ct CSA), and closed porosity [Po (cl)]. (d) AST-120 prevented body weight loss in the CKD-MBD mice. (e) AST-120 prevented the increase in serum creatinine (Cr), calcium (Ca), Pi, indoxyl sulfate (IS), and PCS levels in CKD mice. (f) CKD-induced changes in bone structure were attenuated by AST-120 treatment, with improvements in Ct BV/TV, Ct Th, Ct CSA, and Po (cl). Data are presented as means  $\pm$  SEM ( $n = 5$ ). Analysis was tested by 1-way analysis of variance. \* $P < 0.05$ , \*\* $P < 0.01$ , \*\*\* $P < 0.001$ , and \*\*\*\* $P < 0.0001$  versus the control (CTL) group. NS, not significant.

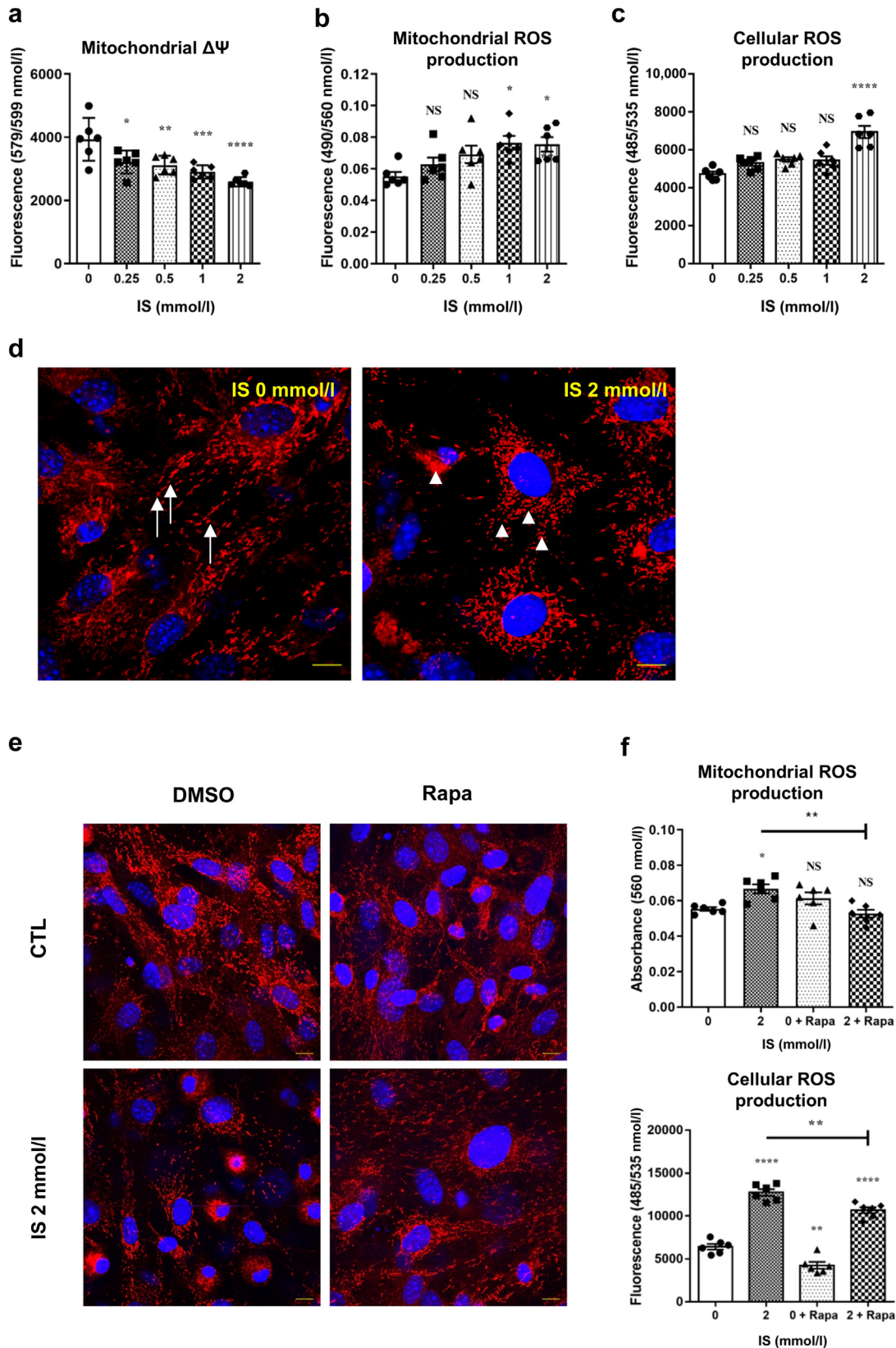


**Figure 9 | Rapamycin (Rapa) reduces reactive oxygen species (ROS) production and rescues indoxyl sulfate (IS)-induced mitochondrial structural abnormality in IS-treated primary osteoblasts. (a)** Decreased mitochondria  $\Delta\Psi$  in IS-treated osteoblasts. **(b)** Increased mitochondrial and **(c)** cellular ROS production by osteoblasts treated with varying concentrations of IS. **(d)** Representative confocal images of primary osteoblasts stained with MitoTracker Red CMXRos (Thermo Fisher Scientific). In control cultures, the mitochondrial network (continued)

models, whereas osteoblasts isolated from CKD-MBD mice mineralized their matrix poorly and expressed lower levels of *Alpl*, *Phospho1*, and *Spp1* (Supplementary Figure S8).

## DISCUSSION

It is well-established that CKD-MBD is associated with poor bone health, but many aspects of the pathophysiology remain unclear. Therefore, to obtain an improved understanding of the biological processes disrupted during the development of ROD, we completed an initial RNA-seq study on cortical bone from a rodent model of CKD-MBD. Various pathways and functions associated with bone metabolism/remodelling that were altered in the CKD-MBD mice were identified. These included disordered osteoclast resorption and extracellular matrix structure and organization, which are recognized to be involved in the etiology of ROD.<sup>17,21,22</sup> However, altered osteoblast or osteocyte mitochondrial function has not previously been reported and warranted further study.

This novel observation in bone is in keeping with previous reports in which mitochondria dysfunction has been associated with pre-CKD kidney diseases.<sup>34</sup> Oxidative stress may be involved, but due to their many integrated functions in addition to their indispensability for cellular respiration and oxidative phosphorylation, the precise nature of the mitochondrial insult remains obscure.<sup>35</sup> While the kidney is particularly susceptible to oxidative stress due to its high energy demands, mitochondria are also essential for maintaining the balance between osteogenesis and bone resorption.<sup>36</sup> Altered mitochondrial function (e.g., mitophagy, fusion, fission, and biogenesis) is associated with decreased bone mass, and mitophagy-focused studies have reported that irregular mitophagy via decreased PINK or PARKIN leads to impaired osteogenic differentiation.<sup>37–39</sup> Impaired autophagic flux noted in osteoblasts and osteocytes of ATG7 null mice may explain the observed lower bone mass, reduced remodeling, and fewer osteocyte projections.<sup>40,41</sup> This study also revealed impaired osteocyte dendritic projections in the cortical bone of CKD-MBD mice. An altered dendritic network would disrupt osteocyte interactions with both osteoblasts and osteoclasts and thereby contribute to the development of ROD.<sup>42</sup> Furthermore, accumulating mitochondrial DNA mutations in mice results in the premature onset of aging-related phenotypes, including osteoporosis and vertebrae compression fractures.<sup>43–45</sup> Corroborating clinical data are limited, but mitochondrial DNA point mutations, including the common m3234A>G are associated with decreased bone mass and strength and severe osteoporosis.<sup>46,47</sup> The causative insults are likely to be complex, but oxidative stress stimulates osteoclast formation and inhibits

osteoblast differentiation via increased sclerostin and the downregulation of Wnt/ $\beta$ -catenin signalling.<sup>45,48,49</sup>

From the RNA-seq data of this study, we speculated that impaired mitophagy in CKD-MBD bones would lead to the retention of damaged mitochondria and could explain the decreased oxidative phosphorylation and contribute to the etiology of ROD. However, the reduced mitophagy, as implied by the RNA-seq data, is at odds with the increased PARKIN protein and mitolysosomes noted in the CKD-MBD *mito-QC* mice. An explanation for this apparent paradox is undoubtedly complex but may be based on the pretext that changes in gene function (protein levels) can be extrapolated from changes in transcript levels.<sup>50</sup> Indeed, in the aging murine kidney, mRNA transcript levels have been reported to be a poor proxy for protein abundance, which may be a consequence of changes in translational efficiency and/or protein turnover.<sup>51</sup> This phenomenon is not uncommon in CKD and aging animal studies focused on renal physiology.<sup>52,53</sup> This disconnect between transcript and protein levels was further emphasized when the expression of established mitophagy regulators in CKD-MBD bone were quantified. In CKD-MBD mouse bone, increased TOMM20 and the preservation of ATG7 and p62/SQSTM1 levels are inconsistent with their recognized roles in the mitophagy process and are indicative of dysfunctional mitophagy.<sup>54–56</sup> The key observation of increased mitolysosomes in the osteocytes of mice fed an adenine-supplemented diet was also observed in a second model (5/6 Nx) of CKD-MBD. While the greater number of mitolysosomes implies increased mitophagy and high baseline turnover, this observation may be misleading due to the possibility of slower degradation of mitolysosomes at the autophagosome stage. A compromised ability to efficiently remove damaged mitochondria as a consequence of dysfunctional mitophagy has been reported previously in a number of nonskeletal organs.<sup>57–59</sup> The increased mitolysosome number observed in CKD-MBD mice persisted in *ex vivo* osteoblasts. Their differentiation and ability to mineralize their matrix were also impaired, suggesting that epigenetic changes may contribute to the altered function of osteoblasts from animals with and patients with CKD-MBD.<sup>60–62</sup>

To determine the driver for the altered mitophagy noted in the bones of the CKD-MBD mice we considered both weight loss and caloric restriction because they can influence cellular metabolism and mitophagy, respectively.<sup>63,64</sup> This explanation is however unlikely because while the nephrectomized mice presented with altered mitolysosome numbers, their body weight and food intake were normal. Rather, we focused on uremic toxins because of their known ability to damage mitochondria and impair autophagic flux.<sup>30,31</sup> The effects of IS

←  
**Figure 9** | (continued) appeared as long thread-like tubular structures (left panel, arrows), whereas those treated with IS (2 mmol/l) had a swollen, rounded morphology (right panel, arrowheads). (e) Abnormally shaped mitochondria in IS-treated cells (2 mmol/l) were restored by adding rapamycin (75 nmol/l). (f) Mitochondrial and cellular ROS production was decreased by osteoblasts treated with 0 or 2 mmol/l IS  $\pm$  Rapa. Bar = 10  $\mu$ m. The data are represented as the mean  $\pm$  SEM (n = 6). \**P* < 0.05, \*\**P* < 0.01, \*\*\**P* < 0.001, and \*\*\*\**P* < 0.0001 versus nontreated control (CTL) group (0 mmol/l). DMSO, dimethylsulfoxide; max, maximum; NS, not significant. To optimize viewing of this image, please see the online version of this article at [www.kidney-international.org](http://www.kidney-international.org).

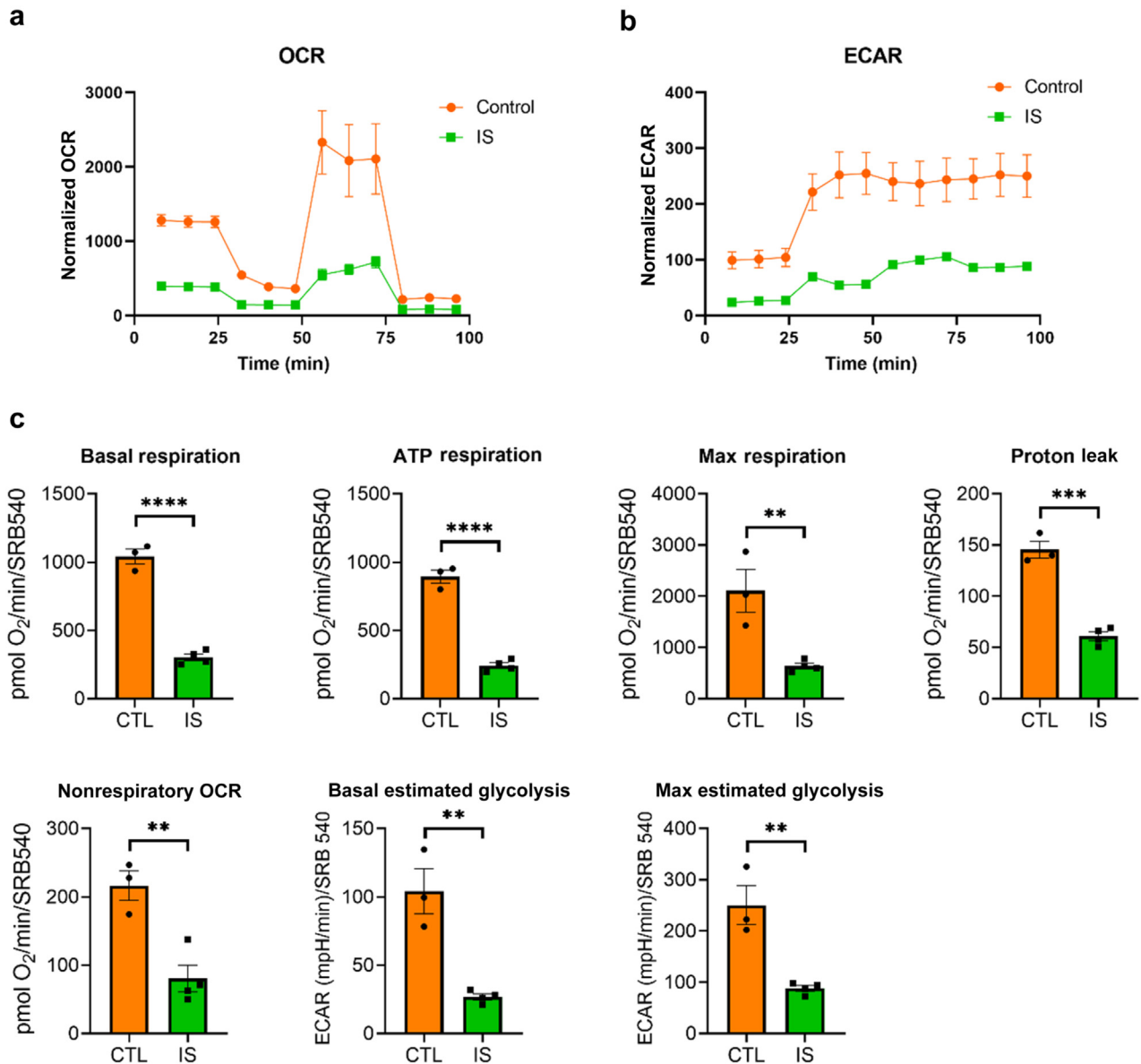


**Figure 10 | The effects of indoxyl sulfate (IS) on oxidative phosphorylation and glycolysis in primary osteoblasts.** Cells were treated in the presence and absence of IS (0 versus 2 mmol/l) for 7 days. (a,b) Mitochondrial oxygen consumption rate (OCR) and extracellular acidification rate (ECAR) in primary osteoblasts following the addition of oligomycin, carbonyl cyanide 4-(trifluoromethoxy) phenylhydrazone (FCCP), and rotenone–antimycin A to target the electron transport chain. Optimal amounts of FCCP was 1.5  $\mu$ mol/l for the controls (CTL) and 3  $\mu$ mol/l for IS. (c) From the OCR and ECAR data, basal respiration, adenosine triphosphate (ATP)-linked respiration, maximal respiration, proton leak, nonrespiratory OCR, basal estimated glycolysis, and maximal estimated glycolysis were all decreased in the IS-treated cells. The data are represented as the mean  $\pm$  SEM (n = 3). \*\* $P$  < 0.01, \*\*\* $P$  < 0.001, and \*\*\*\* $P$  < 0.0001 versus nontreated CTL group (0 mmol/l).

and PCS on osteoblast mitochondria morphology and mitochondria number are consistent with aberrant mitophagy. The increased p62/SQSTM1 and decreased PARKIN and LC3-II also suggest altered mitophagy, but the decreased PARKIN protein is at odds with what is noted in the CKD-MBD mice. This suggests that the effects of IS alone do not fully mimic the *in vivo* situation where other serum factors altered in CKD-MBD may mitigate the actions of uremic toxins on the mitophagy process. Moreover, although mitochondrial damage was observed in IS-treated cells, there was less LC3 punctate/LC3-II within damaged mitochondria, implying there is

reduced PARKIN to signal the autophagosomes. However, as rapamycin reversed the effects of IS on PARKIN, LC3-II, p62/SQSTM1, and punctate LC3, it raises rapamycin and other mitochondria-targeted approaches as a potential pharmacological intervention to manipulate mitochondrial function within cells and reduce CKD-related bone disorders.<sup>57,65,66</sup> Rapamycin, an inhibitor of mammalian target of rapamycin, is a drug clinically used for immunosuppressive, and antitumor purposes; however, its application to augment mitophagy in the complex pathophysiology of ROD may be limited due to its harmful impact on bone formation.<sup>67</sup>

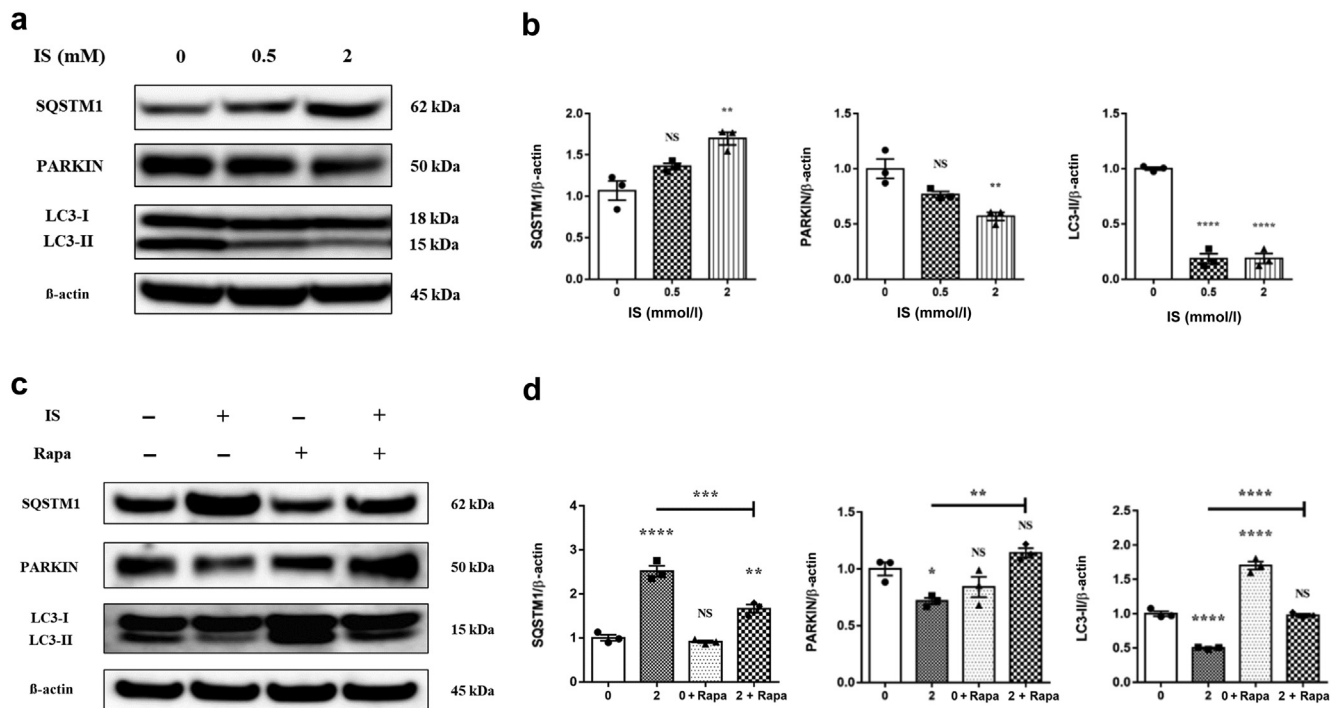


**Figure 11 | Rapamycin (Rapa) reverses the adverse effects of indoxyl sulfate (IS) on primary osteoblast mitophagy.** The expression and quantification of mitophagy regulators by primary osteoblasts treated with increasing concentrations of IS (0, 0.5, and 2 mmol/l) for 7 days. (a,b) IS (0–2 mmol/l) increased the expression of SQSTM1 but decreased the expression of PARKIN (an E3 ubiquitin ligase that promotes mitophagy) and light chain 3 (LC3)-II. (c,d) Rapamycin reversed the effects of IS on the expression of SQSTM1, PARKIN, and LC3-II. The signal intensity was normalized to  $\beta$ -actin and set at 1 for the control cultures (no IS; n = 3). Significance was calculated by 1-way analysis of variance with *post hoc* Tukey multiple comparisons tests. \* $P < 0.05$ , \*\* $P < 0.01$ , and \*\*\*\* $P < 0.0001$  versus untreated control group (0 mmol/l). NS, not significant.

We have speculated that the increased ROS production by mitochondria in bone cells in response to uremic toxins may underpin the altered mitophagy noted in this study. Uremic toxins accumulate in tissues and serum of patients with CKD and have been implicated in the earlier adynamic bone disease phase of ROD, which is characterized by skeletal PTH resistance.<sup>68–70</sup> Uremic toxins inhibit osteoblast differentiation and matrix synthesis and alter bone’s chemical composition, resulting in impaired biomechanical properties and increased fragility.<sup>68,71,72</sup> They may promote these bone pathologies by deregulating mitochondrial metabolism, mass, and dynamics via the induction of oxidative stress by activating reduced NAD phosphate oxidase.<sup>73,74</sup> Disrupted oxidative phosphorylation in IS-treated osteoblasts was noted in this study, as was an accumulation of p62/SQSTM1 and reduced LC3-II protein, which together exemplify impaired mitophagy. The ability of MitoQ, a mitochondria-targeted antioxidant and ROS inhibitor,<sup>75</sup> to mitigate the uremic toxin-induced mitochondrial changes and improve bone health provides evidence of a causal link between altered mitophagy and the development of ROD. This is in agreement with previous murine studies, which have shown MitoQ to be beneficial for skeletal health. MitoQ maintains bone mineral density and bone breaking strength in db/db mice fed a high fat diet.<sup>76</sup> It also influences the progression of osteoarthritis during aging, but intriguingly it does not alter the progression of age-

induced bone loss.<sup>77,78</sup> The causal link between altered mitophagy and the development of ROD was further advanced by our studies with AST-120, an oral adsorbent of uremic toxins.<sup>79</sup> The reduction in both serum IS and PCS, as observed in this study, will reduce oxidative stress and suppress mitochondrial dysfunction and such a mechanism has been proposed to explain the ability of AST-120 to slow CKD progression.<sup>69,80</sup> Clinical studies examining the ability of AST-120 to minimize, delay, or prevent ROD have not been reported, but previous rodent studies have reported that AST-120 can suppress the progression of adynamic bone disease in uremic rats.<sup>68,81</sup> These data support the tenet that uremic toxins damage mitochondria through oxidative stress, impact mitophagic function in bone cells, and contribute to the ROD phenotype.

This body of work provides persuasive evidence that altered osteoblast or osteocyte mitochondrial function has a major impact on the development of ROD and is consistent with the emerging role of the osteocyte in CKD.<sup>82</sup> While not the focus of this study, reports indicate that altered mitochondrial function may explain some of the CKD comorbidities. Muscle wasting is a severe complication of CKD and probably contributes to the increased risk of falls. Experimental evidence suggests impaired mitochondrial metabolism is a crucial mechanism linking kidney dysfunction with sarcopenia.<sup>83,84</sup>

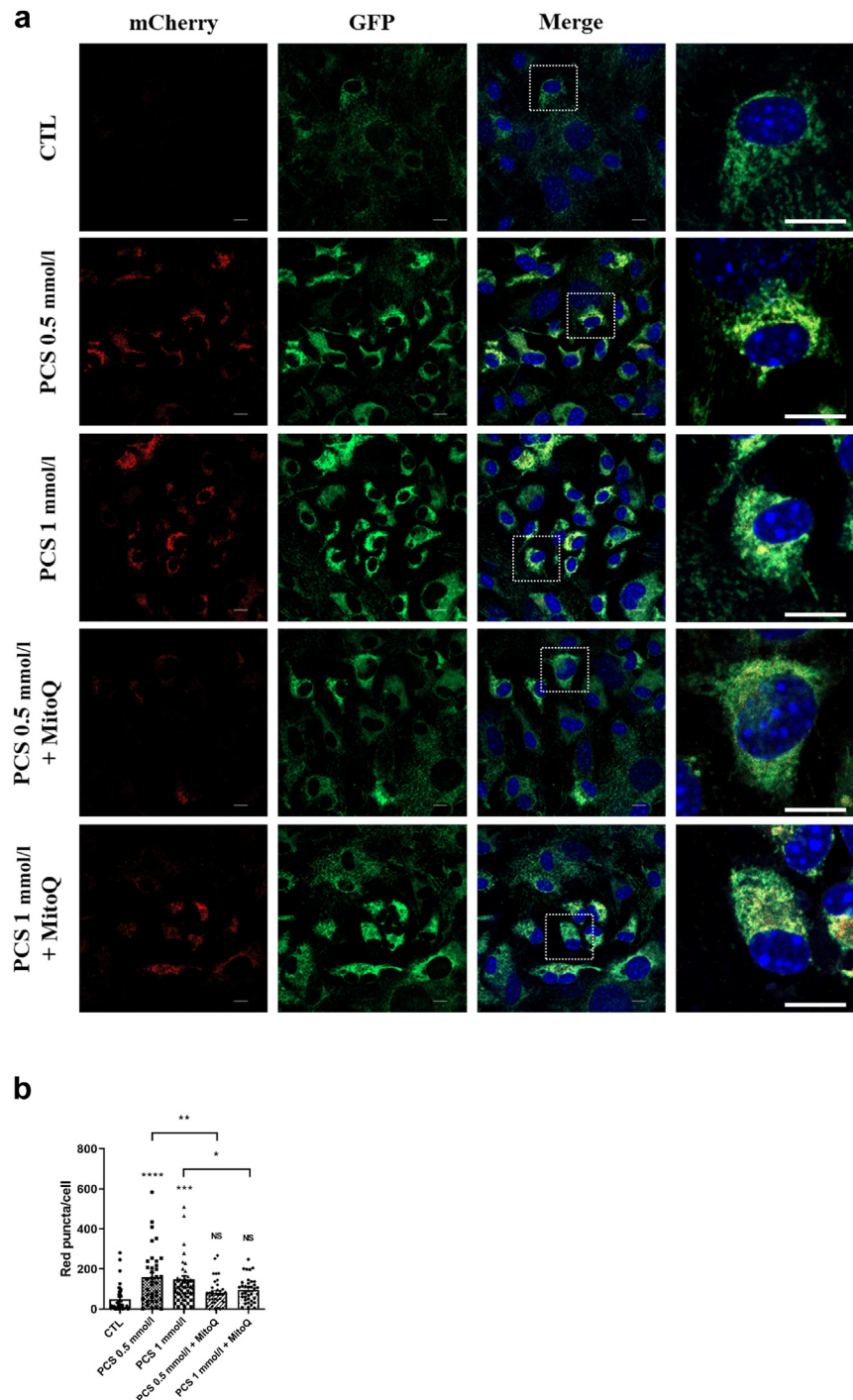


**Figure 12 | Increased mitolysosome number by p-cresyl sulfate (PCS) was prevented with MitoQ.** (a) Representative immunofluorescence images of mitolysosomes in osteoblasts from *mito*-QC mice treated with PCS at 0.5 mmol/l and 1 mmol/l concentrations, with or without MitoQ treatment (0.5  $\mu$ mol/l). Red mitophagic puncta (mCherry) were identified and the merged images show colocalization of mitochondria and mitolysosomes. (b) The number of red puncta per osteoblast was increased by PCS treatment but normalized by MitoQ cotreatment (9 cells per 5 sections per well, n = 4). Bar = 10  $\mu$ m. The data are represented as the mean  $\pm$  SEM. Significance was calculated by 1-way analysis of variance with *post hoc* Tukey multiple comparisons tests. \* $P$  < 0.05, \*\* $P$  < 0.01, \*\*\* $P$  < 0.001, and \*\*\*\* $P$  < 0.0001 versus untreated control (CTL) group (0 mmol/l). GFP, green fluorescent protein; NS, not significant. To optimize viewing of this image, please see the online version of this article at [www.kidney-international.org](http://www.kidney-international.org).

Moreover, the protein levels of various mitophagy mediators such as BNIP3, p62, LC3-II, PARKIN, and PINK1 are altered in mitochondria isolated from muscle tissues

from patients with CKD, which may account for the poor muscle mitochondrial oxidative capacity in patients with CKD.<sup>57,85,86</sup> Interestingly, L-carnitine and teneligliptin, a

**Table 1 | Expression of mitophagy regulators in both *in vivo* and *in vitro* models of CKD**

	CKD gene (Figure 3)	CKD protein (Figure 5)	IS effect (Figure 11)	IS + Rapa effect (Figure 11)	Expected protein effect in normal mitophagy <sup>65,87–89</sup>
PARKIN	Decreased	Increased	Decreased	Reversed	Increased
SQSTM1	Decreased	No change	Increased	Reversed	Decreased
ATG7	No change	No change/decreased	Not known	Not known	Increased
LC3-II	Decreased	Not known	Decreased	Reversed	Increased
TOMM20	No change	Increased	Not known	Not known	Decreased

LC3, light chain 3; PARKIN, an E3 ubiquitin ligase that promotes mitophagy; TOMM20, a subunit of the mitochondrial translocase of the outer membrane complex.

DPP4 inhibitor, normalize muscle mitophagy markers and reduce CKD-induced muscle atrophy in mice.<sup>66</sup>

In summary, using an RNA-seq study of bones from a CKD-MBD mouse model we have identified altered cellular mechanisms implicated in the etiology of ROD. This and follow-up studies revealed evidence of mitochondrial dysfunction and repressed mitophagy within osteoblasts and osteocytes (Table 1).<sup>65,87–89</sup> Because mitochondria are critical for osteoblast and osteocyte function, and mitochondrial respiratory chain dysfunction in osteoblasts results in accelerated bone loss, we propose that the altered uremic toxin levels characteristic of CKD-MBD impair mitochondrial function and contribute to the development of ROD.

**DISCLOSURE**

All the authors declared no competing interests.

**DATA STATEMENT**

All data are available in the main text or in the [Supplementary Material](#). The RNA-seq data supporting the findings of this study are openly available at NCBI Gene Expression Omnibus (GEO) under accession number (PRJNA1181626).

**ACKNOWLEDGMENTS**

We wish to thank Elaine Seawright, Mahéva Vallet, Bob Fleming, and Graeme Robertson for technical assistance; Rongling Wang, Oliver Lin, Tsung-Han Lin, Cheng Wen Hsu, and Thomas Tan for experimental help; and Lance Cih-Jen Lin for helpful discussions on the manuscript drafts. We thank the staff of the Biological Research Facility at the University of Edinburgh for providing animal support, Colin Wood for help with serum analysis, and Scott Maxwell for histological assistance. The human femur tissues were collected with the help of research nurse Fiona Stewart at the Royal Infirmary of Edinburgh, University of Edinburgh.

**FUNDING STATEMENT**

This work was supported by the Ministry of Science and Technology (MOST), Taiwan (113-2314-B-016-051-MY3 and 112-2314-B-016-041-MY3) to S-NH and Y-JH and Tri-Service General Hospital, Taiwan (TSGH\_D\_113138 and TSGH\_D\_113137) to S-NH and Y-JH. We also thank the Biotechnology and Biological Sciences Research Council (BBSRC) for Institute Strategic Programme Grant Funding (BBS/E/RL/230001C and BBS/E/D/10002071) to CF, LAS, VEM, KP, and TCF; the Medical Research Council (MR/V033506/1 and MR/R022240/2) for funding to KAS; and a Wellcome Trust Investigator Award (100981/Z/13/Z) to RCN and NMM.

**AUTHOR CONTRIBUTIONS**

S-NH, Y-JH, KP, LAS, VEM, KAS, and CF were involved in the conceptualization of the study. S-NH, KE, SD, RC, and IL determined the methodology of the study. S-NH, CF, KP, TCF, LAS, and NMM performed formal analyses. CF, Y-JH AKA, NMM, and TCF provided resources. S-NH, KP, and CF wrote the original draft of this manuscript. All authors were involved in writing and reviewing the final edit. S-NH was in charge of visualization of this study. KAS, LAS, VEM, and CF supervised this study. S-NH, Y-JH, and CF acquired funding. All authors read and approved the final manuscript.

Supplementary material is available online at [www.kidney-international.org](http://www.kidney-international.org).

**REFERENCES**

- Patel SS, Kimmel PL, Singh A. New clinical practice guidelines for chronic kidney disease: a framework for K/DOQI. *Semin Nephrol.* 2002;22:449–458.
- Hwang SJ, Tsai JC, Chen HC. Epidemiology, impact and preventive care of chronic kidney disease in Taiwan. *Nephrology.* 2010;15(suppl 2):3–9.
- Lu KC, Wu CC, Yen JF, et al. Vascular calcification and renal bone disorders. *ScientificWorldJournal.* 2014;2014:637065.
- Gracioli FG, Neves KR, Barreto F, et al. The complexity of chronic kidney disease-mineral and bone disorder across stages of chronic kidney disease. *Kidney Int.* 2017;91:1436–1446.
- Moe S, Drüeke T, Cunningham M, et al. Definition, evaluation, and classification of renal osteodystrophy: a position statement from Kidney Disease: Improving Global Outcomes (KDIGO). *Kidney Int.* 2006;69:1945–1953.
- Palmer SC, Hayen A, Macaskill P, et al. Serum levels of phosphorus, parathyroid hormone, and calcium and risks of death and cardiovascular disease in individuals with chronic kidney disease: a systematic review and meta-analysis. *JAMA.* 2011;305:1119–1127.
- Covic A, Kothawala P, Bernal M, et al. Systematic review of the evidence underlying the association between mineral metabolism disturbances and risk of all-cause mortality, cardiovascular mortality and cardiovascular events in chronic kidney disease. *Nephrol Dial Transplant.* 2009;24:1506–1523.
- Ketteler M, Block GA, Evenepoel P, et al. Executive summary of the 2017 KDIGO Chronic Kidney Disease-Mineral and Bone Disorder (CKD-MBD) Guideline Update: what’s changed and why it matters. *Kidney Int.* 2017;92:26–36.
- Hou Y-C, Lu C-L, Lu K-C. Mineral bone disorders in chronic kidney disease. *Nephrology.* 2018;23:88–94.
- Locklin RM, Khosla S, Turner RT, et al. Mediators of the biphasic responses of bone to intermittent and continuously administered parathyroid hormone. *J Cell Biochem.* 2003;89:180–190.
- Fei Y, Xiao L, Hurley MM. The impaired bone anabolic effect of PTH in the absence of endogenous FGF2 is partially due to reduced ATF4 expression. *Biochem Biophys Res Commun.* 2011;412:160–164.
- Watanabe K, Tominari T, Hirata M, et al. Indoxyl sulfate, a uremic toxin in chronic kidney disease, suppresses both bone formation and bone resorption. *FEBS Open Bio.* 2017;7:1178–1185.
- Yamamoto S, Fukagawa M. Uremic toxicity and bone in CKD. *J Nephrol.* 2017;30:623–627.
- Popkov VA, Silachev DN, Zalevsky AO, et al. Mitochondria as a source and a target for uremic toxins. *Int J Mol Sci.* 2019;20:3094.

15. Shyu JF, Liu WC, Zheng CM, et al. Toxic effects of indoxyl sulfate on osteoclastogenesis and osteoblastogenesis. *Int J Mol Sci.* 2021;22:11265.
16. Lang F, Leibrock C, Pandya AA, et al. Phosphate homeostasis, inflammation and the regulation of FGF-23. *Kidney Blood Press Res.* 2018;43:1742–1748.
17. Hsu SN, Stephen LA, Dillon S, et al. Increased PHOSPHO1 expression mediates cortical bone mineral density in renal osteodystrophy. *J Endocrinol.* 2022;254:153–167.
18. Levey AS, Coresh J, Balk E, et al. National Kidney Foundation practice guidelines for chronic kidney disease: evaluation, classification, and stratification. *Ann Intern Med.* 2003;139:137–147.
19. Freeman TC, Horsewell S, Patir A, et al. Graphia: a platform for the graph-based visualisation and analysis of high dimensional data. *PLoS Comput Biol.* 2022;18:e1010310.
20. Mazzaferro S, Cianciolo G, De Pascalis A, et al. Bone, inflammation and the bone marrow niche in chronic kidney disease: what do we know? *Nephrol Dial Transplant.* 2018;33:2092–2100.
21. Misof BM, Blouin S, Roschger P, et al. Bone matrix mineralization and osteocyte lacunae characteristics in patients with chronic kidney disease—mineral bone disorder (CKD-MBD). *J Musculoskelet Neuronal Interact.* 2019;19:196–206.
22. Wesseling-Perry K. Bone disease in pediatric chronic kidney disease. *Pediatr Nephrol.* 2013;28:569–576.
23. Woods GN, Ewing SK, Sigurdsson S, et al. Chronic kidney disease is associated with greater bone marrow adiposity. *J Bone Miner Res.* 2018;33:2158–2164.
24. Stubbs JR, He N, Idiculla A, et al. Longitudinal evaluation of FGF23 changes and mineral metabolism abnormalities in a mouse model of chronic kidney disease. *J Bone Miner Res.* 2012;27:38–46.
25. Kühl I, Miranda M, Atanassov I, et al. Transcriptomic and proteomic landscape of mitochondrial dysfunction reveals secondary coenzyme Q deficiency in mammals. *eLife.* 2017;6:e30952.
26. Han S, Zhang M, Jeong YY, et al. The role of mitophagy in the regulation of mitochondrial energetic status in neurons. *Autophagy.* 2021;17:4182–4201.
27. McWilliams TG, Prescott AR, Allen GF, et al. mito-QC illuminates mitophagy and mitochondrial architecture in vivo. *J Cell Biol.* 2016;214:333–345.
28. Gao J, Qin A, Liu D, et al. Endoplasmic reticulum mediates mitochondrial transfer within the osteocyte dendritic network. *Sci Adv.* 2019;5:eaaw7215.
29. Pankiv S, Clausen TH, Lamark T, et al. p62/SQSTM1 binds directly to Atg8/LC3 to facilitate degradation of ubiquitinated protein aggregates by autophagy. *J Biol Chem.* 2007;282:24131–24145.
30. Wojtaszek E, Oldakowska-Jedynak U, Kwiatkowska M, et al. Uremic toxins, oxidative stress, atherosclerosis in chronic kidney disease, and kidney transplantation. *Oxid Med Cell Longev.* 2021;2021:6651367.
31. Rodrigues SD, Santos SS, Meireles T, et al. Uremic toxins promote accumulation of oxidized protein and increased sensitivity to hydrogen peroxide in endothelial cells by impairing the autophagic flux. *Biochem Biophys Res Commun.* 2020;523:123–129.
32. Bielas J, Herbst A, Widjaja K, et al. Long term rapamycin treatment improves mitochondrial DNA quality in aging mice. *Exp Gerontol.* 2018;106:125–131.
33. Cheema NJ, Cameron JM, Hood DA. Effect of rapamycin on mitochondria and lysosomes in fibroblasts from patients with mtDNA mutations. *Am J Physiol Cell Physiol.* 2021;321:C176–C186.
34. Brooks C, Wei Q, Cho SG, et al. Regulation of mitochondrial dynamics in acute kidney injury in cell culture and rodent models. *J Clin Invest.* 2009;119:1275–1285.
35. Galvan DL, Green NH, Danesh FR. The hallmarks of mitochondrial dysfunction in chronic kidney disease. *Kidney Int.* 2017;92:1051–1057.
36. Yan C, Shi Y, Yuan L, et al. Mitochondrial quality control and its role in osteoporosis. *Front Endocrinol.* 2023;14:1077058.
37. Gao J, Feng Z, Wang X, et al. SIRT3/SOD2 maintains osteoblast differentiation and bone formation by regulating mitochondrial stress. *Cell Death Differ.* 2018;25:229–240.
38. Lee S-Y, An H-J, Kim JM, et al. PINK1 deficiency impairs osteoblast differentiation through aberrant mitochondrial homeostasis. *Stem Cell Res Ther.* 2021;12:589.
39. Marycz K, Kornicka K, Maređziak M, et al. Equine metabolic syndrome impairs adipose stem cells' osteogenic differentiation by predominance of autophagy over selective mitophagy. *J Cell Mol Med.* 2016;20:2384–2404.
40. Piemontese M, Onal M, Xiong J, et al. Low bone mass and changes in the osteocyte network in mice lacking autophagy in the osteoblast lineage. *Sci Rep.* 2016;6:24262.
41. Li H, Li D, Ma Z, et al. Defective autophagy in osteoblasts induces endoplasmic reticulum stress and causes remarkable bone loss. *Autophagy.* 2018;14:1726–1741.
42. Dallas SL, Prideaux M, Bonewald LF. The osteocyte: an endocrine cell ... and more. *Endocr Rev.* 2013;34:658–690.
43. Dobson PF, Dennis EP, Hipps D, et al. Mitochondrial dysfunction impairs osteogenesis, increases osteoclast activity, and accelerates age related bone loss. *Sci Rep.* 2020;10:11643.
44. Miyazaki T, Iwasawa M, Nakashima T, et al. Intracellular and extracellular ATP coordinately regulate the inverse correlation between osteoclast survival and bone resorption. *J Biol Chem.* 2012;287:37808–37823.
45. Kobayashi K, Nojiri H, Saita Y, et al. Mitochondrial superoxide in osteocytes perturbs canalicular networks in the setting of age-related osteoporosis. *Sci Rep.* 2015;5:9148.
46. Langdahl JH, Frederiksen AL, Hansen SJ, et al. Mitochondrial point mutation m.3243A>G associates with lower bone mineral density, thinner cortices, and reduced bone strength: a case-control study. *J Bone Miner Res.* 2017;32:2041–2048.
47. Varanasi SS, Francis RM, Berger CEM, et al. Mitochondrial DNA deletion associated oxidative stress and severe male osteoporosis. *Osteoporos Int.* 1999;10:143–149.
48. Bartell SM, Kim H-N, Ambrogini E, et al. FoxO proteins restrain osteoclastogenesis and bone resorption by attenuating H2O2 accumulation. *Nat Commun.* 2014;5:3773.
49. Almeida M, Han L, Martin-Millan M, et al. Oxidative stress antagonizes Wnt signaling in osteoblast precursors by diverting beta-catenin from T cell factor- to forkhead box O-mediated transcription. *J Biol Chem.* 2007;282:27298–27305.
50. Liu Y, Beyer A, Aebersold R. On the dependency of cellular protein levels on mRNA abundance. *Cell.* 2016;165:535–550.
51. Takemon Y, Chick JM, Gerdes Gyuricza I, et al. Proteomic and transcriptomic profiling reveal different aspects of aging in the kidney. *eLife.* 2021;10:e62585.
52. Feng D, Ngoc C, Henley N, et al. Characterization of matricellular protein expression signatures in mechanically diverse mouse models of kidney injury. *Sci Rep.* 2019;9:16736.
53. Sharifian R, Okamura DM, Denisenko O, et al. Distinct patterns of transcriptional and epigenetic alterations characterize acute and chronic kidney injury. *Sci Rep.* 2018;8:17870.
54. Narendra D, Kane LA, Hauser DN, et al. p62/SQSTM1 is required for Parkin-induced mitochondrial clustering but not mitophagy; VDAC1 is dispensable for both. *Autophagy.* 2010;6:1090–1106.
55. Komatsu M, Waguri S, Koike M, et al. Homeostatic levels of p62 control cytoplasmic inclusion body formation in autophagy-deficient mice. *Cell.* 2007;131:1149–1163.
56. Yamada T, Dawson TM, Yanagawa T, et al. SQSTM1/p62 promotes mitochondrial ubiquitination independently of PINK1 and PRKN/parkin in mitophagy. *Autophagy.* 2019;15:2012–2018.
57. Mito T, Vincent AE, Fajt J, et al. Mosaic dysfunction of mitophagy in mitochondrial muscle disease. *Cell Metab.* 2022;34:197–208.e195.
58. Mary A, Eysert F, Checler F, et al. Mitophagy in Alzheimer's disease: molecular defects and therapeutic approaches. *Mol Psychiatry.* 2023;28:202–216.
59. Hwang S, Disatnik M-H, Mochly-Rosen D. Impaired GAPDH-induced mitophagy contributes to the pathology of Huntington's disease. *EMBO Mol Med.* 2015;7:1307–1326.
60. Chen NX, O'Neill KD, Allen MR, et al. Low bone turnover in chronic kidney disease is associated with decreased VEGF-A expression and osteoblast differentiation. *Am J Nephrol.* 2015;41:464–473.
61. Pereira RC, Delany AM, Khouzam NM, et al. Primary osteoblast-like cells from patients with end-stage kidney disease reflect gene expression, proliferation, and mineralization characteristics ex vivo. *Kidney Int.* 2015;87:593–601.
62. Martin A, Kawaguchi R, Wang Q, et al. Chromatin accessibility and epigenetic deoxyribose nucleic acid (DNA) modifications in chronic kidney disease (CKD) osteoblasts: a study of bone and osteoblasts from pediatric patients with CKD. *JBMR Plus.* 2024;8:z1ad015.

63. Tareen SHK, Kutmon M, de Kok TM, et al. Stratifying cellular metabolism during weight loss: an interplay of metabolism, metabolic flexibility and inflammation. *Sci Rep.* 2020;10:1651.
64. Mehrabani S, Bagherniya M, Askari G, et al. The effect of fasting or calorie restriction on mitophagy induction: a literature review. *J Cachexia Sarcopenia Muscle.* 2020;11:1447–1458.
65. Bao J, Chen Z, Xu L, et al. Rapamycin protects chondrocytes against IL-18-induced apoptosis and ameliorates rat osteoarthritis. *Aging.* 2020;12:5152–5167.
66. Enoki Y, Watanabe H, Arake R, et al. Potential therapeutic interventions for chronic kidney disease-associated sarcopenia via indoxyl sulfate-induced mitochondrial dysfunction. *J Cachexia Sarcopenia Muscle.* 2017;8:735–747.
67. Xian L, Wu X, Pang L, et al. Matrix IGF-1 maintains bone mass by activation of mTOR in mesenchymal stem cells. *Nat Med.* 2012;18:1095–1101.
68. Iwasaki Y, Kazama JJ, Yamato H, et al. Accumulated uremic toxins attenuate bone mechanical properties in rats with chronic kidney disease. *Bone.* 2013;57:477–483.
69. Asai M, Kumakura S, Kikuchi M. Review of the efficacy of AST-120 (KREMEZIN®) on renal function in chronic kidney disease patients. *Ren Fail.* 2019;41:47–56.
70. Chen NX, O'Neill KD, Wilson HE, et al. The uremic toxin indoxyl sulfate decreases osteocyte RANKL/OPG and increases wnt inhibitor RNA expression that is reversed by PTH. *JBMR Plus.* 2024;9:ziae136.
71. Kim Y-H, Kwak K-A, Gil H-W, et al. Indoxyl sulfate promotes apoptosis in cultured osteoblast cells. *BMC Pharmacol Toxicol.* 2013;14:60.
72. Tanaka H, Iwasaki Y, Yamato H, et al. Cresyl sulfate induces osteoblast dysfunction through activating JNK and p38 MAPK pathways. *Bone.* 2013;56:347–354.
73. Sun CY, Cheng ML, Pan HC, et al. Protein-bound uremic toxins impaired mitochondrial dynamics and functions. *Oncotarget.* 2017;8:77722–77733.
74. Lee W-C, Li L-C, Chen J-B, et al. Indoxyl sulfate-induced oxidative stress, mitochondrial dysfunction, and impaired biogenesis are partly protected by vitamin C and N-acetylcysteine. *ScientificWorldJournal.* 2015;2015:620826.
75. Murphy MP, Smith RA. Targeting antioxidants to mitochondria by conjugation to lipophilic cations. *Ann Rev Pharmacol Toxicol.* 2007;47:629–656.
76. Li J, He W, Liao B, et al. FFA-ROS-P53-mediated mitochondrial apoptosis contributes to reduction of osteoblastogenesis and bone mass in type 2 diabetes mellitus. *Sci Rep.* 2015;5:12724.
77. Poudel SB, Ruff RR, Yildirim G, et al. Development of primary osteoarthritis during aging in genetically diverse UM-HET3 mice. *Arthritis Res Ther.* 2024;26:118.
78. Poudel SB, Frikha-Benayed D, Ruff RR, et al. Targeting mitochondrial dysfunction using methylene blue or mitoquinone to improve skeletal aging. *Aging.* 2024;16:4948–4964.
79. Nakagawa N, Hasebe N, Sumitomo K, et al. An oral adsorbent, AST-120, suppresses oxidative stress in uremic rats. *Am J Nephrol.* 2006;26:455–461.
80. Konishi K, Nakano S, Tsuda S, et al. AST-120 (Kremezin) initiated in early stage chronic kidney disease stunts the progression of renal dysfunction in type 2 diabetic subjects. *Diabetes Res Clin Pract.* 2008;81:310–315.
81. Iwasaki Y, Yamato H, Nii-Kono T, et al. Administration of oral charcoal adsorbent (AST-120) suppresses low-turnover bone progression in uremic rats. *Nephrol Dial Transplant.* 2006;21:2768–2774.
82. Albrecht LV, Pereira RC, Salusky IB. All the might of the osteocyte: emerging roles in chronic kidney disease. *Kidney Int.* 2023;104:910–915.
83. Gamboa JL, Billings FT 4th, Bojanowski MT, et al. Mitochondrial dysfunction and oxidative stress in patients with chronic kidney disease. *Physiol Rep.* 2016;4:e12780.
84. Gortan Cappellari G, Semolic A, Ruozi G, et al. Unacylated ghrelin normalizes skeletal muscle oxidative stress and prevents muscle catabolism by enhancing tissue mitophagy in experimental chronic kidney disease. *FASEB J.* 2017;31:5159–5171.
85. Kestenbaum B, Gamboa J, Liu S, et al. Impaired skeletal muscle mitochondrial bioenergetics and physical performance in chronic kidney disease. *JCI Insight.* 2020;5:e133289.
86. Zhang YY, Gu LJ, Huang J, et al. CKD autophagy activation and skeletal muscle atrophy—a preliminary study of mitophagy and inflammation. *Eur J Clin Nutr.* 2019;73:950–960.
87. Guo X, Zhang W, Wang C, et al. IRGM promotes the PINK1-mediated mitophagy through the degradation of Mitofilin in SH-SY5Y cells. *FASEB J.* 2020;34:14768–14779.
88. Yang Y-Y, Gong D-J, Zhang J-J, et al. Diabetes aggravates renal ischemia-reperfusion injury by repressing mitochondrial function and PINK1/Parkin-mediated mitophagy. *Am J Physiol Renal Physiol.* 2019;317:F852–F864.
89. Berezhnov AV, Soutar MP, Fedotova EI, et al. Intracellular pH modulates autophagy and mitophagy. *J Biol Chem.* 2016;291:8701–8708.